Journal of Structural Geology 33 (2011) 1569–1594

Contents lists available at SciVerse ScienceDirect

Journal of Structural Geology

journal homepage: www.elsevier.com/locate/jsg

Telescoping of isotherms beneath the South Tibetan Detachment System, Mount Everest Massif

R.D. Law[a,*], M.J. Jessup[b], M.P. Searle[c], M.K. Francsis[a], D.J. Waters[c], J.M. Cottle[d]

[a] Department of Geosciences, Virginia Tech, Blacksburg, VA 24061, USA
[b] Department of Earth and Planetary Sciences, University of Tennessee, Knoxville, TN 37996, USA
[c] Department of Earth Sciences, University of Oxford, Oxford OX1 3PR, UK
[d] Department of Earth Science, University of California, Santa Barbara, CA 93106-9630, USA

ARTICLE INFO

Article history:
Received 10 May 2011
Received in revised form
7 September 2011
Accepted 9 September 2011
Available online 16 September 2011

Keywords:
Mount Everest
Detachment
Quartz fabrics
Deformation temperatures
Strain
Strain rate

ABSTRACT

Petrologic and microstructural/crystal fabric data indicate that isotherms recorded in Greater Himalayan Series (GHS) schists and gneisses in the footwall to the South Tibetan Detachment System (STDS) have undergone extreme telescoping during penetrative flow associated with southward extrusion of the GHS. In the Rongbuk Valley, to the north of Mount Everest, we have made three vertical sampling traverses from the STDS down into the GHS and estimated temperatures associated with penetrative deformation using the opening angles of quartz c-axis fabrics measured on dynamically recrystallized grains. From north to south, the deformation temperature data indicate apparent thermal field gradients of 369, 385 and 420 °C per km for our three traverses, traced over a maximum vertical sampling distance of 0.5 km. Adopting a differential flow path model, simple geometric analysis using sections drawn parallel to the local transport direction indicates that detachment-parallel transport magnitudes of 25–170 km are needed to explain the extreme telescoping of isotherms in the immediate footwall to the STDS, depending on assumed original geothermal gradient, dip of detachment, etc. These particle transport estimates are similar to those previously calculated from barometry data of GHS rocks in the Everest region and are compatible with channel flow models for extrusion and exhumation of the GHS.

1. Introduction

Within the central-eastern sector of the Himalayan orogen the highest grade metamorphic rocks, referred to as the Greater Himalayan Series (GHS), are exposed in the Greater Himalayan slab, a 20–30 km thick northward-dipping tectonic unit of metasedimentary and granitic rocks pervasively deformed under mid-crustal conditions (Fig. 1). The slab is bounded along the base by the south-directed Main Central Thrust (MCT), and along the top by the South Tibetan Detachment System (STDS) of north-directed normal faults (Fig. 2a) that separate the metamorphic and anatectic core of the Himalaya from the essentially unmetamorphosed sedimentary Tethyan passive margin sedimentary sequence to the north. Structural studies and geochronology indicate that thrusting and normal faulting on the margins of the GHS are broadly synchronous (Godin et al., 2006 and references therein). Both thrust and normal faults initiated synchronously with Miocene prograde metamorphism and melting, and have moved episodically since then. Beginning in Early Miocene time, south – southwestward extrusion of the GHS between the MCT and STDS has had a profound influence on the geologic and geomorphic evolution of the Himalaya (Hodges et al., 2001; Law et al., 2006 and papers therein). The regional scale geometries of the thrust and normal faults bounding the slab are now reasonably well known, and considerable research has been done on documenting shear sense indicators and components of simple and pure shear along the upper and lower surfaces of the slab, and constraining the early stage PTt paths of rocks within the slab.

It has long been known that while metamorphic isograds along the base of the slab are inverted, isograds at the top of the slab are right way up (e.g. Searle and Rex, 1989). The lower and upper surfaces of the slab are ductile shear zones, up to 1.5–2.0 km wide, in which the isograds have been telescoped (or condensed) by S- and N-directed general shear, respectively (Fig. 2b,c). These isograds are defined by metamorphic mineral assemblages of Himalayan (Oligocene-Miocene) age that locally either predate or are coeval with the intense penetrative shearing and crystal plastic deformation observed at outcrop along the upper and lower surfaces of the slab. However, although numerous field- and microstructures-based studies have addressed the kinematic

* Corresponding author. Tel.: +1 540 231 6685.
E-mail address: rdlaw@vt.edu (R.D. Law).

0191-8141/$ – see front matter © 2011 Elsevier Ltd. All rights reserved.
doi:10.1016/j.jsg.2011.09.004

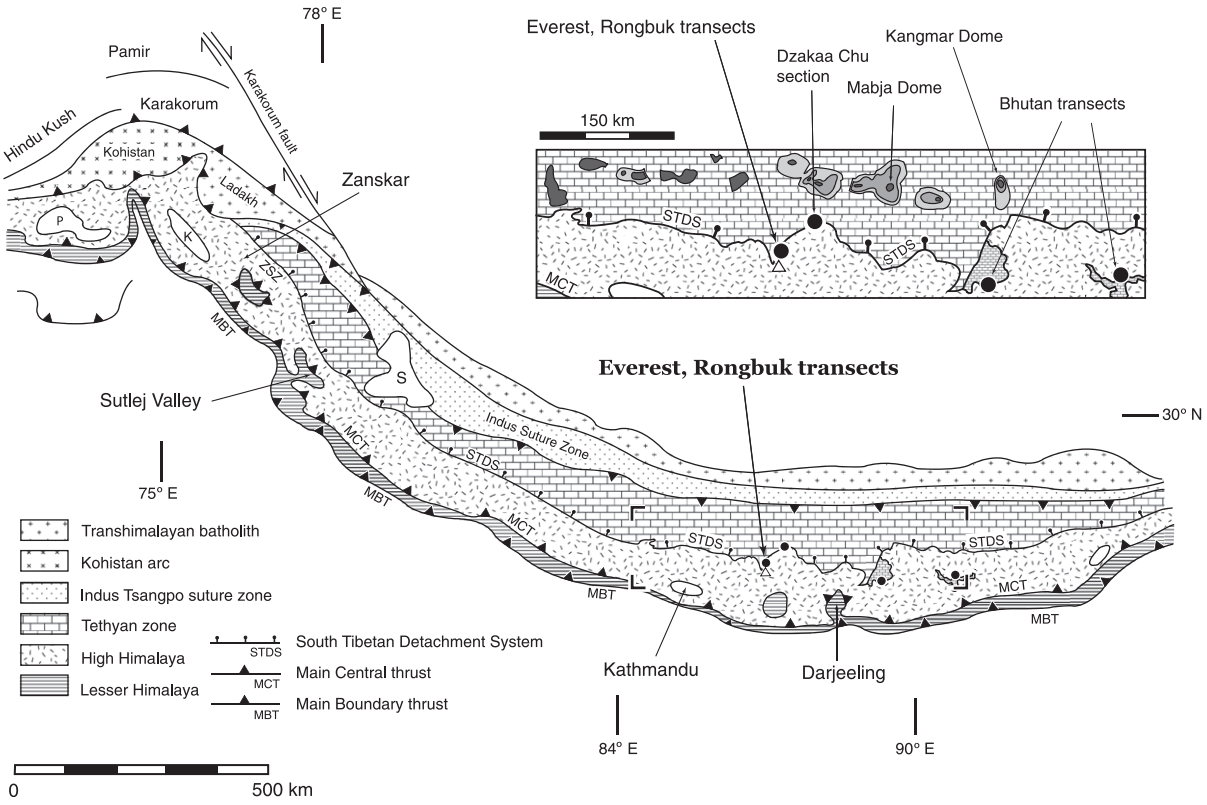

Fig. 1. Simplified geologic sketch map of the Himalaya showing distribution of the main lithotectonic elements and main areas discussed in text; adapted from Burchfiel et al. (1992) and Searle et al. (2008). The Greater Himalayan Series (Slab) is bounded below by the Main Central thrust (MCT) and above by the South Tibetan Detachment System (STDS). MBT, Main Boundary thrust; ZSZ, Zanskar shear zone. Positions of Kathmandu, Sutlej (S), Kashmir (K) and Peshawar (P) basins are indicated. Inset-map indicates positions of North Himalayan Gneiss Domes (including Kangmar and Mabja Domes discussed in text); dark shading – crystalline cores to gneiss domes, medium and light gray shading – high grade and low-grade metamorphic rocks surrounding domes (after Burchfiel et al., 1992; Wagner et al., 2010). Positions of the Dzakaa Chu transect across the STDS (Cottle et al., 2007, 2011), and transects across klippen of the STDS in western Bhutan (Kellett et al., 2010) are also indicated.

evolution of the STDS, its thermal structure is less well understood. This is partly due to the relative scarcity of metamorphic index minerals in many sections across the STDS.

In this paper we present new quantitative data on flow stresses, deformation temperatures, strain rates and telescoping of isotherms associated with northward-directed (normal sense) flow at the top of the GHS, and the potential implications of this telescoping of isotherms for magnitude of transport of these mid-crustal rocks in the immediate footwall of the STDS. Deformation temperatures are inferred from the opening angles of quartz c-axis fabrics that are demonstrably related to crystal plastic deformation associated with southward-directed extrusion and exhumation of the GHS. Thus, isotherms based on these deformation temperature data developed during exhumation. In contrast, mapped isograds are based on metamorphic mineral assemblages that may have developed either before or during exhumation.

The data were collected from the Rongbuk area on the north (Tibetan) side of the Everest Massif (Fig. 3) where two low angle normal faults bound the upper surface of the GHS, the earlier and structurally lower Lhotse detachment and the later and structurally higher Qomolangma detachment (Searle, 1999, 2003). These data and their interpretation build upon preliminary accounts of fabric-based deformation temperatures reported by Law et al. (2004, 2008) from reconnaissance sampling of GHS rocks in the footwall to the Lhotse detachment in the Rongbuk area, and complement earlier companion studies by Searle et al. (2003, 2006), Law et al. (2004) and Jessup et al. (2006, 2008) on the structural geology, flow vorticities, thermobarometry and geochronology of the GHS in the Everest region.

2. Geology of the Rongbuk – Mount Everest area

2.1. Tectonic setting

On the north side of the Mount Everest Massif two major detachments have been mapped in the sidewalls of the Rongbuk valley southwards to Changtse and Mount Everest, the upper brittle Qomolangma detachment (QD) and the lower ductile Lhotse detachment (LD), which merge towards the north into one large-scale shear zone (Cottle et al., 2007).

The LD dips gently (<15°) towards the NE and, as originally defined, is a distinct ductile high strain zone that marks a metamorphic break between amphibolite-facies GHS metasedimentary rocks and leucogranites below and greenschist-facies (Everest Series) metasedimentary rocks above (Searle, 1999). However, more recent detailed thermobarometric results from samples collected above the East Rongbuk glacier (Waters et al., 2006; Waters unpublished data) and at the base of the Lhotse wall (Jessup et al., 2008) indicate maximum temperatures of c. 650 °C in pelitic Everest Series rocks immediately above the LD, and suggest that the LD – at least in the Everest area – may mark the upper limit of anatectic leucogranites, but not an unequivocal break in metamorphic grade.

Metamorphic grade decreases up structural section in the overlying Everest Series with greenschist-facies rocks being exposed on the NE Ridge of Mount Everest (Waters, unpublished data). Below the summit of Mount Everest these pelitic Everest Series rocks are overlain by coarse-grained dynamically recrystallized marbles of the Yellow Band. The Yellow Band is in turn

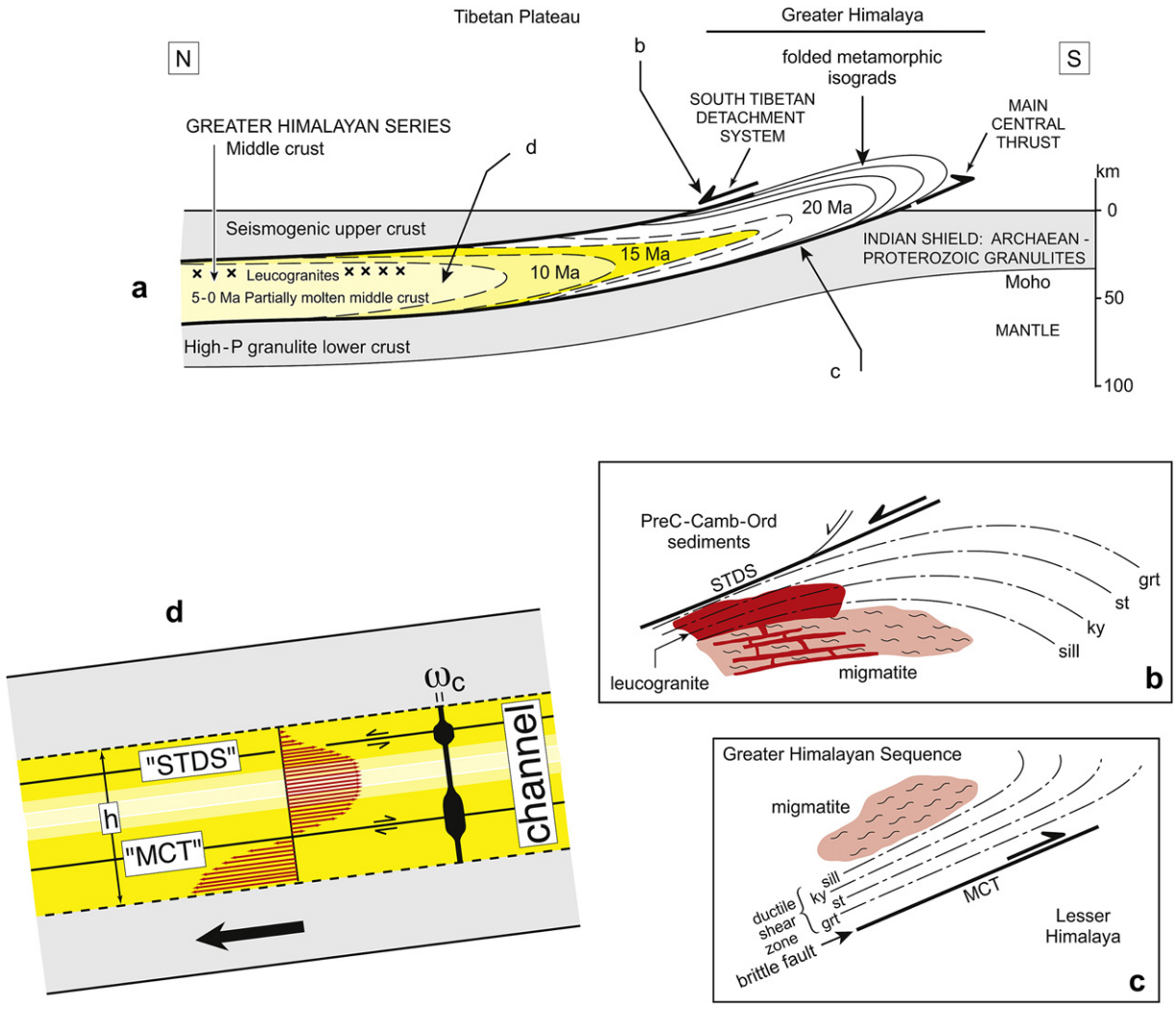

Fig. 2. Channel Flow model of ductile extrusion of a partially molten mid-crustal slab (GHS) in the Himalaya bounded above by a low-angle normal sense ductile shear zone and fault (South Tibetan Detachment System) and below by an SW-vergent ductile shear zone and thrust fault (Main Central thrust). (a) folded metamorphic isograds (based on Zanskar-Kishtwar Himalaya of NW India; Searle and Rex, 1989; Searle et al., 1999) linking the STDS footwall and MCT hanging wall represent 'frozen' 20-15 Ma isograds adjacent to a younger and more active channel of partial melting present beneath southern Tibet today; adapted from Searle et al. (2006, 2007). (b, c) telescoping of isograds in footwall to STDS and hanging wall to MCT; adapted from Searle et al. (2007). (d) hypothetical velocity profile in a Himalayan-type orogenic channel; adapted from Grujic et al. (2002). Vorticity values indicated by width of black bar, with simple shear (Wk = 1) dominated flow in cooler higher viscosity rocks adjacent to STDS and MCT and general shear (Wk <1) in hotter lower viscosity rocks in center of channel.

separated by the Qomolangma detachment (QD) from dominantly fine-grained Ordovician limestones, the Qomolangma Formation, forming the summit pyramid of Mount Everest (Sakai et al., 2005, see also Myrow et al., 2009 for historical review). Most of these summit strata consist of recrystallized sandy limestone (Jessup et al., 2006; their Fig. 6a). Raman spectroscopy of carbonaceous material in the summit limestones indicate maximum burial temperatures of ~338 °C (Cottle, 2007).

The QD dips more steeply to the north and east than the LD (Searle, 2003) with the intervening Everest Series defining a northward-tapering tectonic wedge of greenschist-amphibolite facies rocks separating unmetamorphosed – weakly metamorphosed Ordovician limestones above from underlying amphibolite facies schists, gneisses and leucogranites of the GHS. To the north of Mount Everest in the walls of the Rongbuk Valley the QD and LD merge in to a single brittle-ductile detachment separating unmetamorphosed, probably also Ordovician age, limestones of the Tethyan Zone from the underlying high grade rocks of the GHS.

Nowhere along the QD can footwall rocks be matched with hanging-wall rocks and an absolute minimum of 34 km of dip-slip displacement along the QD has been proposed (Burchfiel et al., 1992). Based on barometry of metamorphic mineral assemblages in GHS rocks collected on the Nepal side of the Mount Everest Massif, Searle et al. (2002, 2003) have estimated that dip-slip displacement on the combined strands of the STDS may have been on the order of 100–200 km, depending on the dip (5–10°) of the detachment during exhumation of the GHS footwall rocks. In the Everest area the minimum age of ductile shearing along the LD is constrained at ~17 Ma, while brittle faulting on the QD must be younger than 16 Ma (Hodges et al., 1998; Murphy and Harrison, 1999; Searle et al., 2003).

The Tertiary thermal histories of both the GHS and Everest Series rocks in the Everest region are defined by clockwise Pressure–Temperature (P–T) paths. As reviewed by Cottle et al. (2009, 2011), the GHS records an early kyanite-grade metamorphism (550–560 °C and 8–10 kbar) ranging in age from 39 to 32 Ma, followed by sillimanite grade metamorphism (650–750 °C and

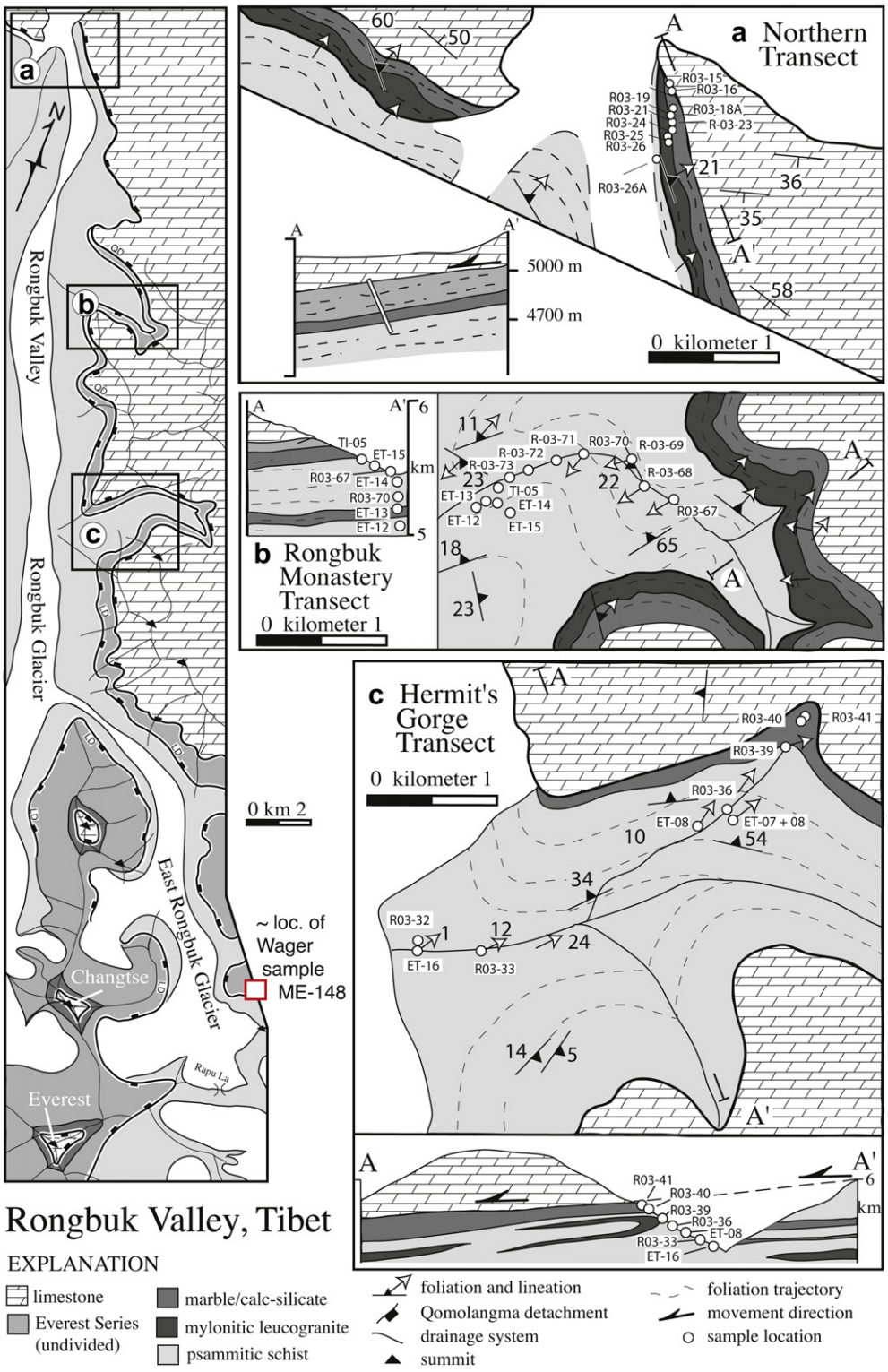

Fig. 3. Simplified geologic map of Rongbuk valley, Tibet. Insets (a–c) are enlargements of detailed sample transects. Spatial distribution of samples is also shown on the cross section through each transect. North is oblique to the long axis of the figure. Adapted from Jessup et al. (2006). Position of Everest Series sample ME-148 collected by L.R. Wager in 1933 above East Rongbuk Glacier indicated.

4–7 kbar) at 28–22.6 Ma. In-situ partial melting and formation of leucogranites in the GHS occurred as early as ~25–26 Ma with major phases of pre- to syn-kinematic melting occurring between ~24 and 18 Ma and later syn- to post-kinematic melting at ~22–16 Ma (Cottle et al., 2009). However, diagnostic mineral assemblages needed to define P-T paths have not been recorded in GHS rocks exposed in the Rongbuk area. The pervasive deformation fabrics in these rocks are associated with a top down to the north shear sense (Burchfiel et al., 1992; Carosi et al., 1998; Law et al., 2004) with the component of simple shear increasing structurally

upwards towards the overlying detachment (s) (Jessup et al., 2006). At least at structural distances of >400 m beneath the detachment, top down to the north (normal sense) penetrative deformation in the GHS occurred at close to peak (sillimanite grade) metamorphic temperatures (Law et al., 2004).

Mineral assemblages needed to define P-T conditions in the Everest Series pelites have been recorded within a suite of unoriented samples collected by L.R. Wager in 1933 above the East Rongbuk glacier and on the Northeast Ridge of Mount Everest (Waters et al., 2006; unpublished data). Wager's sample ME-148 collected above the East Rongbuk Glacier at a structural distance of ~100 m above the Lhotse detachment (Fig. 3) contains multiple fabrics, some of which are clearly prograde. Maximum pressures and temperatures of 5.2 kbar and 640 °C are indicated for Everest Series sample ME-148 (Fig. 4); no geochronological data are available. Microstructural relationships indicate that pervasive deformation fabrics in sample ME-148 developed after peak temperature during exhumation and cooling (4.5–2.6 kbar and 640-550 °C) (Waters, unpublished data). Thus penetrative deformation fabrics preserved in both the Everest Series and GHS rocks appear to be associated with exhumation and pervasive shearing associated with normal (top down to the north) sense motion on the various strands of the STDS.

2.2. Geological background to the Rongbuk area

In the Rongbuk area the STDS is marked by a single brittle-ductile detachment marking the merged Qomolangma and Lhotse detachments. In the southern part of the Rongbuk area (Fig. 3b and c) the detachment dips at 3–5° to the NNE (Burchfiel et al., 1992; Murphy and Harrison, 1999; Searle, 2003; Searle et al., 2003) and is marked by a zone of intense shearing some tens of m in width between the Tethyan limestones and underlying metamorphic rocks of the GHS. In the northern part of the area (Fig. 3a) the detachment dips slightly more steeply (~10–15 to the NE) and is marked by a discrete

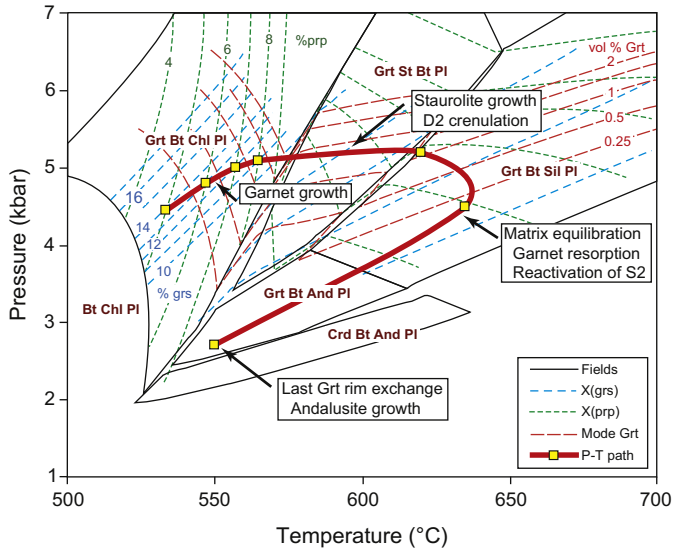

Fig. 4. P–T pseudosection for Everest Series metapelite sample ME-148 showing assemblage fields, composition and mode isopleths for garnet (chemical system MnNCKFMASH), and the clockwise P-T-time trajectory inferred from compositional and microstructural evidence (Waters et al., 2006 and unpublished data). All assemblages contain the additional phases muscovite, quartz and water, and the bulk composition in mole % oxides is SiO_2 62.4, Al_2O_3 16.9, FeO 6.6, MgO 4.5, MnO 0.1, CaO 3.7, Na_2O 2.7, K_2O 3.1, with H_2O in excess. Sample ME-148 was collected by L.R. Wager in 1933 above the East Rongbuk Glacier (Fig. 3; Latitude 28° 02′ 17" N; Longitude 86°, 57′, 46 " E – from *Google Earth*) at ~100 m above the Lhotse detachment of Searle (2003).

structural break between the two units (Carosi et al., 1998; Jessup et al., 2006). The GHS exposed in the eastern walls of the Rongbuk Valley consists of a series of calc-silicate horizons underlain by biotite-rich schists and gneisses that are intruded by leucogranite dykes and sills (Yin and Kuo, 1978; Lombardo et al., 1993; Pognante and Benna, 1993; Carosi et al., 1998; Searle et al., 2003, 2006; Law et al., 2004). Pure calcite marble horizons, sometimes >100 m thick, are locally inter-layered with the schists and gneisses. Sillimanite is present in pelitic units, typically at distances >400 m beneath the detachment. Other indicator metamorphic minerals such as garnet, however, are exceptionally rare in GHS metasedimentary rocks exposed in the Rongbuk area.

The GHS rocks are pervasively foliated with a variably developed mineral stretching lineation. Foliation is gently dipping and associated mineral lineations trend NE-SW. In the Rongbuk area foliation is axial planar to rootless isoclinal folds defined by lithologic banding (Burchfiel et al., 1992; Carosi et al., 1998) and has a gentle (5°) vector-averaged dip towards the NE with associated mineral lineations having a vector-averaged plunge of 4–5° towards the NNE (Fig. 5). In sections cut perpendicular to foliation and parallel to lineations, microstructures indicate a top to the NNE shear sense (Carosi et al., 1998; Law et al., 2004), although conjugate shear bands in some sections indicate a significant pure shear component of deformation.

3. The Rongbuk structural transects

Oriented samples have been collected along three sampling transects in to the footwall of the STDS in the Rongbuk area. From south to north these transects are the Hermit's Gorge, Rongbuk Monastery and Northern transects (Fig. 3). Above all three transects the Qomolangma and Lhotse detachments have essentially merged, and it is uncertain if any unequivocal Everest Series rocks are present immediately above the GHS rocks (Burchfiel et al., 1992; Carosi et al., 1998; Murphy and Harrison, 1999; Searle, 2003). Particularly traced towards the north, sheared Tethyan limestones (detachment hanging wall) rest directly on top of the GHS footwall rocks (e.g. Northern transect; Burchfiel et al., 1992; Carosi et al., 1998; Jessup et al., 2006). Preliminary microstructural, strain, quartz c-axis fabric, deformation temperature and flow vorticity data from the Hermit's Gorge and Rongbuk Monastery transects, together with representative micrographs, were reported by Law et al. (2004), based on a suite of nine reconnaissance samples. A more detailed analysis of flow vorticities for all three transects, based on a significantly larger suite of samples, was subsequently reported by Jessup et al. (2006).

In this paper we focus on documenting variation in deformation temperatures with depth beneath the detachment in GHS metasedimentary rocks and leucogranite sills sampled along all three transects. We also estimate flow stresses and strain rates for the quartz-rich metasedimentary rocks on these transects. Our thermal analyses are based on recording quartz recrystallization regimes and quartz c-axis fabric opening angles, and employ the microstructural and fabric thermometers of Stipp et al. (2002a, b) and Kruhl (1998), respectively, to estimate deformation temperatures associated with penetrative deformation. Our analyses are therefore limited to quartz-rich samples collected along the three transects. Map locations for samples used are indicated in Fig. 3. Vertical positions of samples are given both as altitudes above sea level and as vertical distances beneath the detachment (Supplementary Tables 1 and 2). Due to the gentle dip (3–5°) of the detachment, particularly above the Hermit's Gorge and Rongbuk Monastery transects, these vertical distances correspond, within observational error, to structural distances beneath the detachment. Samples were collected at vertical distances of up to 450 and

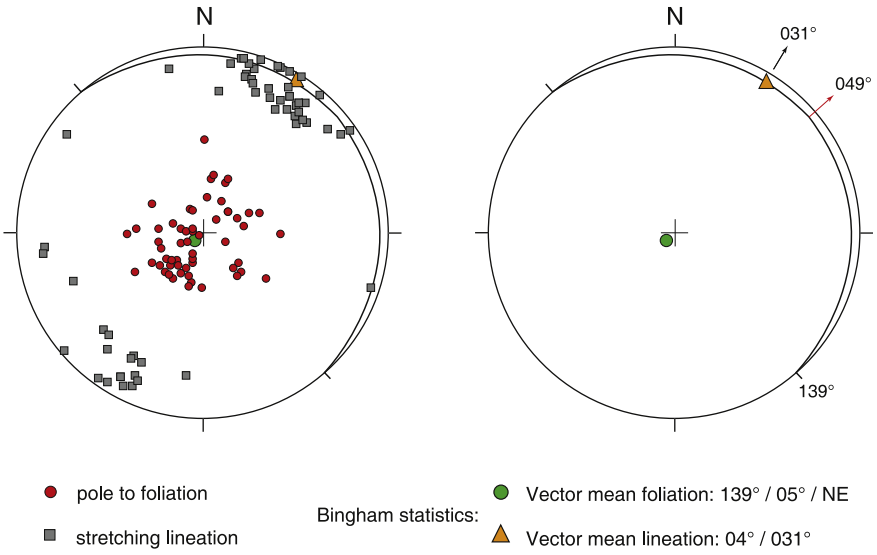

Fig. 5. Foliation and stretching lineation data from the Hermit's Gorge, Rongbuk Monastery and Northern transects; equal-area lower hemisphere projections.

550 m beneath the detachment in the Hermit's Gorge and Rongbuk Monastery transects, respectively. In contrast the Northern transect represents a much shorter exposed profile through the footwall GHS rocks, with samples only being collected to a distance of c. 70 m beneath the detachment. A small correction has been made for detachment dip (10–15°) in estimating distance beneath the detachment for the structurally deeper samples in this transect. It should be noted that incorrect altitudes were given for samples in the original description of the Northern transect by Jessup et al. (2006; their Fig. 10a), although the relative vertical distances between samples were correct.

All microstructural and crystal fabric data are reported from thin sections cut perpendicular to foliation and parallel to lineation. For all oriented samples these data are viewed towards the east such that a top down-to-the N to NNE (i.e. normal sense) motion is indicated by a sinistral shear sense.

3.1. Variation in recrystallization regime, grain size and flow stress of quartz with structural depth

Differential flow stresses associated with plastic deformation in samples from the Rongbuk transects have been estimated using the quartz recrystallized grain size piezometer of Stipp and Tullis (2003) and recently published, experimentally-based, corrections to this piezometer by Holyoke and Kronenberg (2010). Within the uncertainties of their experimental data, the Stipp and Tullis (2003) piezometer has no apparent dependence on temperature, the α–β transition or water content of the quartz (Stipp et al., 2006). However, experimental calibrations for the Stipp and Tullis (2003) piezometer were only carried out up to a maximum grain size of c. 50 microns produced by GBM recrystallization. Stipp et al. (2010) argued that extrapolation of this piezometer to natural grain sizes >120 microns may only yield minimum stress estimates.

Recrystallized grain sizes and flow stress estimates for metasedimentary rocks from the three Rongbuk transects, and their variation with structural distance beneath the detachment, are summarized in Fig. 6 and Supplementary Table 1. In the Rongbuk samples grain size is correlated with recrystallization mechanism, with smaller grains produced by sub-grain rotation and larger grains being produced by grain boundary migration (regimes 2 and 3 of Hirth and Tullis, 1992; corresponding to the SGR and GBM I microstructures of Stipp et al., 2002a,b). Following the analytical procedure of Stipp and Tullis (2003) no correction was made for the 'cut-effect' in estimating grain sizes. Details of these optical thin-section based grain size analyses and associated stress estimates will form the subject of a separate paper. Only average grain sizes for each sample are reported in this paper (Fig. 6a–c; see Supplementary Table 1 for analytical methods used) and these averages are used to estimate flow stresses (Fig. 6d–f).

Quartz recrystallization microstructures are correlated with structural depth beneath the detachment. Microstructural indicators for sub-grain rotation (SGR) are limited to the structurally highest parts of the transects, and are most clearly developed in samples R-03-41, 40 and 39 collected on the Hermit's Gorge transect at < 50 m beneath the detachment (Fig. 6c). Sample R-03-16(2) from the Northern transect (Fig. 6a) also exhibits clear SGR microstructures in a cm-scale leucogranite sill. In these samples, recrystallization of quartz has involved components of both sub-grain rotation and grain boundary migration although grain boundary migration is by far the dominant recrystallization process in quartz-rich domains. Similar microstructures are observed from foliation-parallel quartz-rich layers (probably deformed veins) in Rongbuk Monastery transect sample TI-5 (eroded from an outcrop located at c. 75 m beneath the detachment, see Section 3.4) and Northern Transect samples R-03-15 to 23 collected at <30 m beneath the overlying late brittle detachment surface.

Subgrain rotation is indicated by the presence of fairly equant (15–20 micron diameter) grains in association with larger (30–50 micron) more tabular grains. Grain boundary migration is indicated by sutured grain boundaries, lack of sub-grain development, local mica inclusions, and 50–200 + micron grain sizes. The operation of both recrystallization mechanisms in samples close to the overlying detachment leads to a bimodal distribution of quartz grain sizes, in which the larger grains associated with grain boundary migration are dominant.

In the structurally deeper metasedimentary rocks of all three transects (>50–80 m beneath the detachment) quartz recrystallization appears to be exclusively controlled by grain boundary migration with average recrystallized grain size progressively increasing from c. 90–160 microns (Fig. 6b,c). The interiors of these grains appear to be remarkably strain free with only very rare

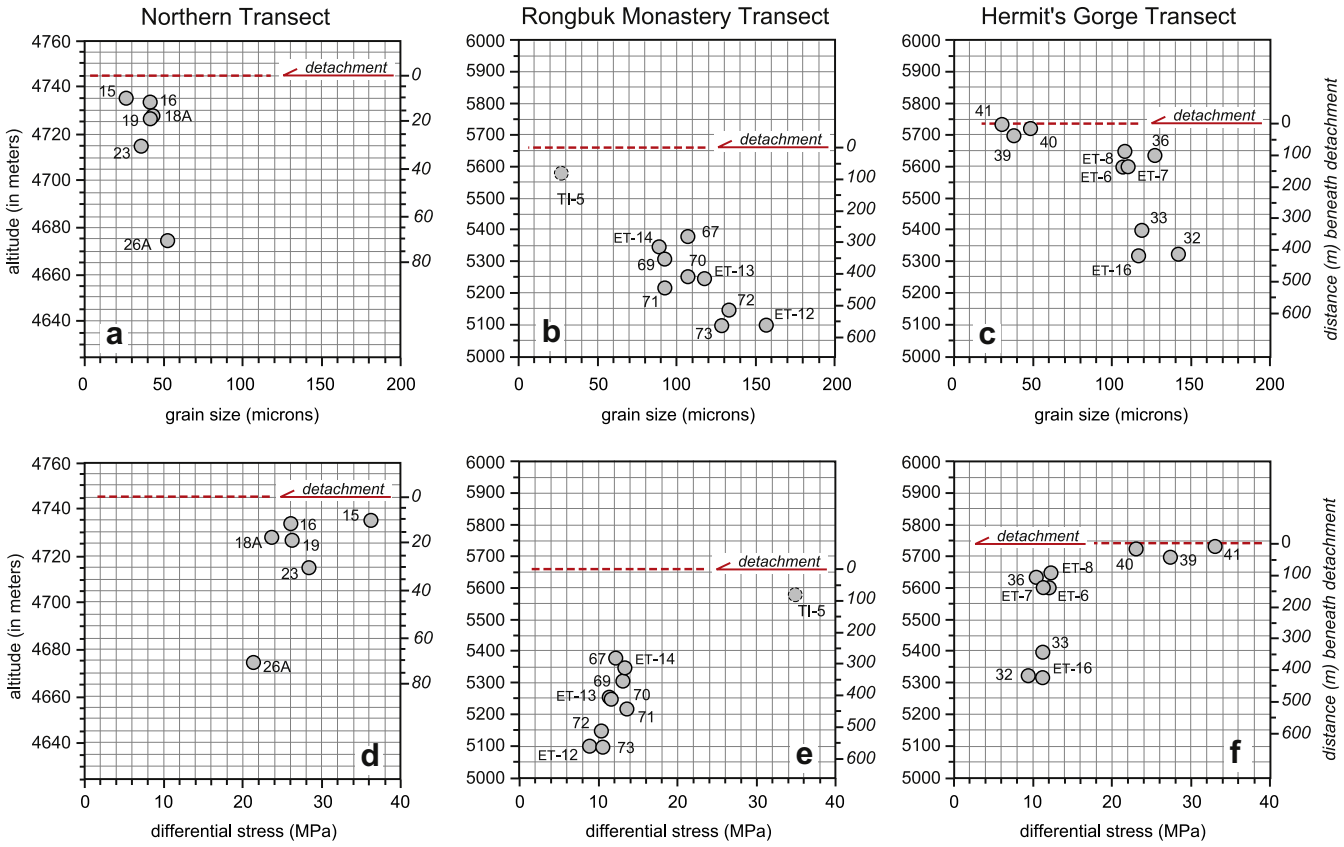

Fig. 6. (a–c) Recrystallized grain size data for GHS metasedimentary rocks from the Northern, Rongbuk Monastery and Hermit's Gorge transects. (d–f) Differential flow stresses (in MPa) estimated from grain size data using piezometer of Stipp and Tullis (2003) with corrections to original piezometer recommended by Holyoke and Kronenberg (2010). Positions of samples beneath the gently dipping detachment indicated both by altitudes above sea level and structural distance beneath detachment; see text for further details. Note different vertical scale used for Northern Transect (a, d). See Fig. 3 for sample locations; grain size and flow stress data are also summarized in Supplementary Table 1.

examples of significant undulose extinction or deformation band development. These "quenched" microstructures indicate rapid exhumation, in agreement with previous isotopic dating studies of the Rongbuk leucogranites (Hodges et al., 1998; Murphy and Harrison, 1999). Pervasive development of undulose extinction and foliation-parallel deformation bands, potentially indicating relatively late-stage lower temperature or higher strain rate deformation, has only been observed in quartz veins from some of the mylonitic leucogranite sills on the Rongbuk Monastery and Northern transects, and in quartz veins from metasedimentary rocks on the Northern transect located close (<30 m) to the overlying brittle detachment.

At depths of 100–550 m beneath the detachment differential stress magnitudes of 10–15 MPa (100–150 bars) are estimated for the Rongbuk Monastery and Hermit's Gorge transects (Fig. 6e,f). In this regime dominated by grain boundary migration recrystallization estimated flow stresses using the Stipp and Tullis (2003) piezometer are relatively insensitive to large changes in grain size. Estimated differential flow stresses increase to c. 15–35 MPa at <50–100 m beneath the detachment (Northern and Hermit's Gorge transects, Fig. 6d,f) where microstructural evidence for components of both sub-grain rotation and grain boundary migration are observed in quartz-rich domains. Whether these recrystallization mechanisms were synchronous, or operated at different times, is unclear. If, for example, sub-grain rotation post-dated grain boundary migration then the average grain sizes used would potentially over-estimate flow stresses associated with earlier deformation, but underestimate stresses associated with later deformation.

3.2. Variation in deformation temperatures with structural depth based on recrystallization regimes

Adopting the microstructural thermometer of Stipp et al. (2002a), deformation temperatures of c. 490–530 °C would be indicated by the combined sub-grain rotation and grain boundary migration recrystallization of quartz observed in samples located close (<30–50 m) to the overlying detachment surfaces(s). This assumes that operation of the two recrystallization mechanisms was synchronous. In structurally deeper metasedimentary rocks, quartz has exclusively recrystallized by grain boundary migration indicating deformation temperatures > c. 530 °C.

High deformation temperatures are also indicated by the deformation of feldspar in these rocks. For example, orthoclase and plagioclase feldspar grains are locally plastically deformed (as indicated by undulose extinction and grain flattening), suggesting deformation temperatures >450–500 °C (Tullis and Yund, 1992; Fitzgerald and Stunitz, 1993). However, in all samples the larger feldspar grains appear to have remained rigid or deformed in a brittle manner, while only the smaller grains exhibit undulose extinction with sutured boundaries between adjacent feldspar grains, suggesting at least limited grain boundary migration (Law et al., 2004).

We interpret the smaller recrystallized quartz grain sizes in the immediate footwall to the detachment as indicating that higher differential flow stresses (Fig. 6) can be supported in these cooler rocks than in the underlying hotter rocks located at greater depths beneath the detachment. Caveats associated with using these microstructures as deformation thermometers are discussed in Section 3.8.

3.3. Quartz c-axis fabrics – asymmetry and variation in opening angles with structural depth

Quartz c-axis fabrics were measured on dynamically recrystallized quartz grains using an optical microscope and Leitz universal stage, with a minimum of 600 grains being measured in each sample. Universal stage data were collected using an *Excel* macro developed by S. Mulcahy at University of California, Davis. Fabrics were contoured using the *Stereoplot* software package developed by N. Mancktelow at ETH, Zurich. Fabrics are displayed on lower hemisphere equal area projections in which the projection plane is oriented perpendicular to foliation and parallel to the NNE-SSW trending stretching lineation; all fabric diagrams are viewed towards the east. Where appropriate, the orientation of microstructures such as shear bands (denoted by bars with arrows) are indicated on the fabric diagrams.

Original point data and contoured c-axis fabrics for each sample from the Hermit's Gorge, Rongbuk Monastery and Northern transects are shown in Figs. 7–9, respectively. For each transect samples are arranged in order of descending structural position. All metasedimentary and leucogranite samples are characterized by transitional Type 1 to Type 2 (Lister, 1977) cross-girdle c-axis fabrics. In all samples these fabrics intersect the penetrative foliation at right angles to the NNE-SSW trending macroscopic mineral lineation, indicating that the lineation has developed parallel to the maximum principal stretching direction associated with plastic deformation. Skeletal analysis (Lister and Williams, 1979) of the contoured fabrics indicates that internal and external fabric asymmetry parameters (Supplementary Fig. 1a) are consistent with a top down to the N shear sense. Data from these skeletal analyses are summarized in Supplementary Fig. 1b–e and Table 2. The only exceptions to the top down to the N shear sense fabric asymmetries are recorded in sample ET-13 (Supplementary Fig. 1b and d) and R-03-26A (Supplementary Fig. 1c, d and e) where some, but not all, fabric asymmetry parameters indicate the opposite shear sense. Even in these two samples, however, a top down to the N shear sense is indicated by shear bands (Figs. 8 and 9). From a tectonics viewpoint, unequivocal documentation of this top down to the N shear sense is critically important because it demonstrates that the crystal fabrics recorded in both the GHS metasedimentary rocks and leucogranites developed during exhumation.

Quartz c-axis fabric opening angles (combined C1 and C2 parameters in Supplementary Fig. 1a) have been proposed as a potential thermometer by Kruhl (1998) with the opening angle increasing as the component of prism [c] slip becomes progressively more important with increasing deformation temperatures (Supplementary Fig. 2; Law et al. (1992); Morgan and Law (2004)). Uncertainties in calculated deformation temperatures using the Kruhl (1998) thermometer have been estimated at ±50 °C. This deformation thermometer offers a potential method for assessing the thermal structure of the Rongbuk GHS rocks in the footwall to the detachment where, as outlined above, appropriate metamorphic mineral assemblages for thermobarometry are generally absent. If valid as a thermometer, this fabrics-based method will yield information on deformation temperatures for the time during exhumation at which plastic deformation (dislocation creep and dynamic recrystallization) ceased and crystallographic fabrics were locked in for individual samples. Caveats associated with using quartz fabric opening angles as a deformation thermometer are discussed in Section 3.8.

The opening angles of c-axis fabrics are plotted against distance beneath the detachment for the three Rongbuk sampling transects in Fig. 10a–c. Opening angles measured in the metasedimentary rocks sampled (gray filled circles in Fig. 10) increase linearly with distance beneath the detachment. Opening angles in the plastically deformed leucogranite sills (triangles in Fig. 10) are always larger than opening angles in adjacent metasedimentary rocks, but the difference in opening angles between leucogranite and adjacent metasedimentary rocks is controlled by the local thickness of the sill. In cases where sills are only 10–20 cm thick, fabric opening angles measured in the centers of the sills are only 1 or 2° larger than in the adjacent metasedimentary rocks (e.g. sample R-03-21, Fig. 10a). In cases where the sills are thicker (ranging from 10s of centimeters to c. 5–15 m) fabric opening angles are 4–6° larger than in the adjacent metasedimentary rocks (e.g. sample ET-15, Fig. 10b; samples R-03-24, 25 and 26, Fig. 10a), with the opening angles increasing towards the center of the sills.

3.4. Variation in deformation temperatures with structural depth based on fabric opening angles

Deformation temperatures indicated by the Kruhl (1998) fabric opening angle thermometer (Supplementary Fig. 2) are plotted against distance beneath the detachment for the three Rongbuk sampling transects in Fig. 10d–f. As dictated by the fabric opening angles, inferred deformation temperatures increase linearly with distance beneath the detachment. Linear regression lines through the deformation temperature data from the metasedimentary rock samples (gray filled circles in Fig. 10) indicate apparent thermal gradients of 420, 385 and 369 °C per km in the Hermit's Gorge, Rongbuk Monastery and Northern transects, respectively. The tectonic implications of this extreme apparent telescoping of isotherms in the footwall to the detachment will be discussed in Section 4 of this paper.

On the Hermit's Gorge transect deformation temperatures within 10–20 m of the overlying detachment are estimated at 480–490 °C, steadily increasing to 625–680 °C at c. 420 m beneath the detachment (Fig. 10f, Supplementary Table 2). This downward increase in deformation temperatures quantified by fabric opening angles is in good agreement with deformation temperature distribution qualitatively indicated by the downward transition in quartz recrystallization regime (sub-grain rotation being limited to the structurally highest samples R-03-41, 40 and 39), topology of quartz c-axis fabrics (Type I to II cross-girdles; Fig. 7) and increasing plasticity of feldspar. These deformation temperatures are also in broad agreement with temperatures indicated by metamorphic mineral assemblages although, as noted above, low-variance mineral assemblages suitable for quantitative thermobarometry are relatively rare in the Rongbuk Valley (Hodges et al., 1992). One pelitic GHS sample with an appropriate mineral assemblage for simultaneous solution of the garnet-biotite and garnet-plagioclase-sillimanite-quartz thermobarometers was collected by Hodges et al. (1992; their sample R74) from the junction between Hermit's Gorge and the Rongbuk valley at the same locality as our sample ET-16, collected at c. 420 m beneath the detachment (Fig. 3). The quartz c-axis fabric opening angle in sample ET-16 indicates a deformation temperature of 625 ± 50 °C (Fig. 10f), in good agreement with calculated 'final equilibration' conditions of 630 °C and 4.6 kbar for sample R74 (Hodges et al., 1992). These temperature and pressure estimates are also very close to those estimated for commencement of exhumation-related grain shape fabric development on the calculated PT path for Wager's sample ME-148 (Fig. 4) collected from the Everest Series rocks above the East Rongbuk Glacier (Fig. 3).

No quartz-rich units were found immediately below the detachment on the Rongbuk Monastery transect where calc-silicate horizons are the dominant unit in the GHS at this structural position. Sample TI-5, a mylonitic epidote amphibolite-facies schist (Law et al., 2004, their Fig. 4c) collected from a talus pile on this transect is characterized by mixed sub-grain

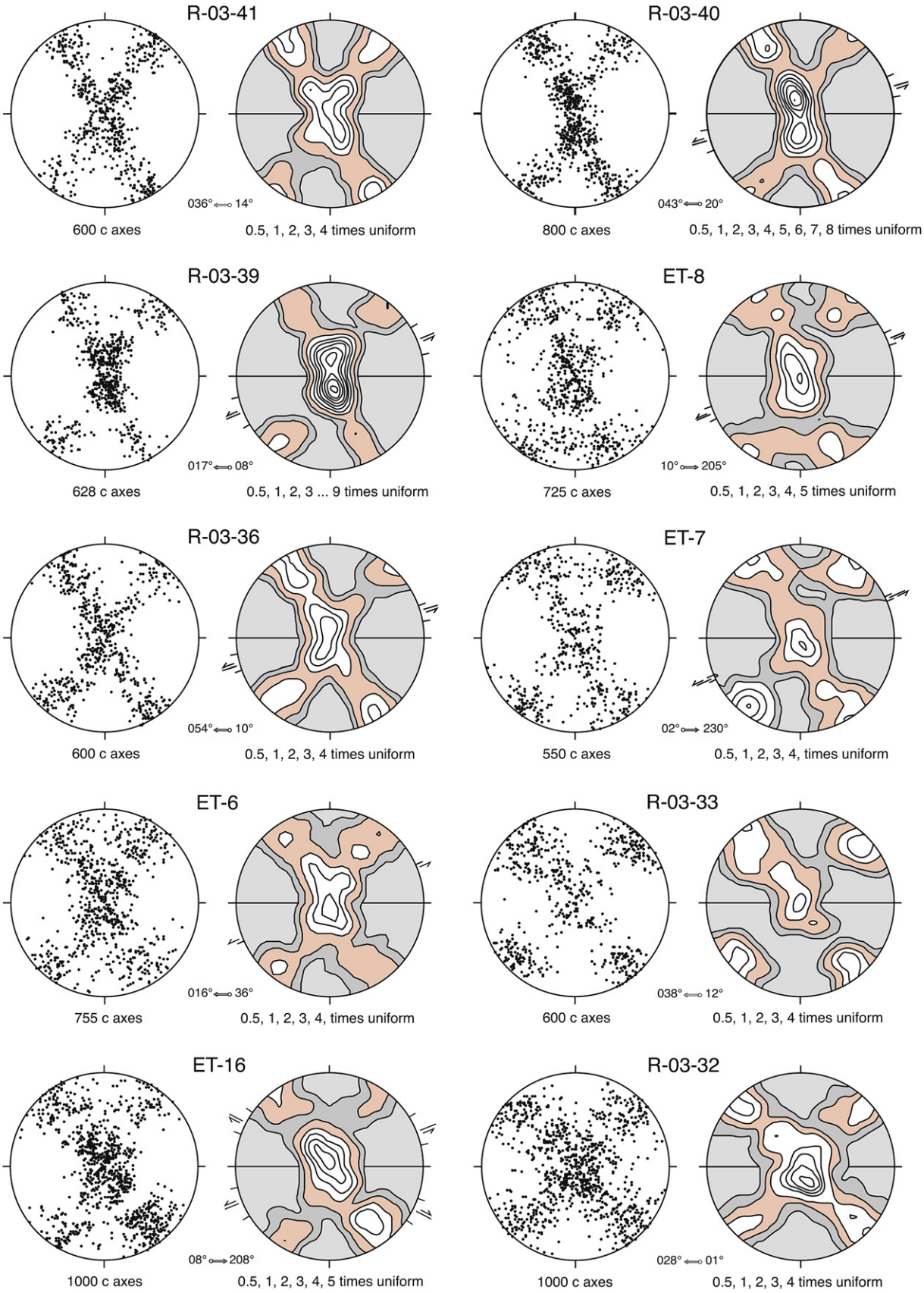

Fig. 7. Optically measured quartz c-axis fabrics for GHS metasedimentary rocks from the Hermit's Gorge Transect. All lower hemisphere equal area projections viewed towards the east and oriented perpendicular to foliation (horizontal line) and parallel to stretching lineation. Fabrics arranged in order of increasing structural distance beneath detachment (see also Figs. 3 and 10). All *in-situ* oriented samples; plunge and trend of lineation, range of shear band orientations and contour intervals indicated for each sample. Skeletal fabric parameter data for these samples are summarized in Supplementary Fig. 1 and Table 2. Fabrics for samples ET-8, ET-7, ET-6 and ET-16 previously described by Law et al. (2004).

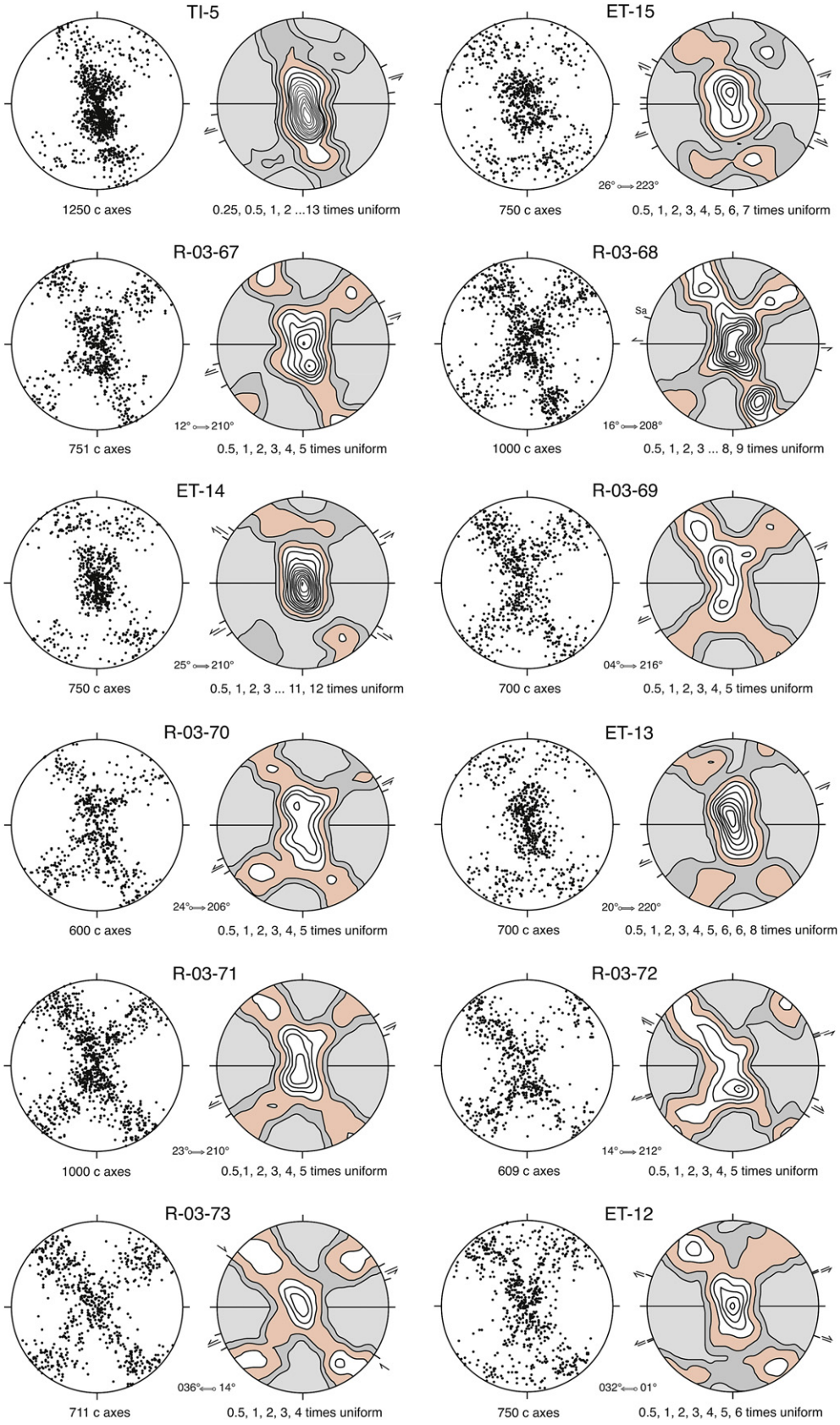

Fig. 8. Optically measured quartz c-axis fabrics for GHS metasedimentary rocks and leucogranite sills (ET-15 and R-03-68) from the Rongbuk Monastery Transect. All lower hemisphere equal area projections viewed towards the east and oriented perpendicular to foliation (horizontal line) and parallel to stretching lineation. Fabrics arranged in order of increasing structural distance beneath detachment (see also Figs. 3 and 10). With the exception of sample TI-5 (see text), all *in-situ* oriented samples; plunge and trend of lineation, range of shear band orientations and contour intervals indicated for each sample. Skeletal fabric parameter data for these samples are summarized in Supplementary Fig. 1 and Table 2. Fabrics for samples TI-5, ET-15, ET-14, ET-13 and ET-12 previously described by Law et al. (2004).

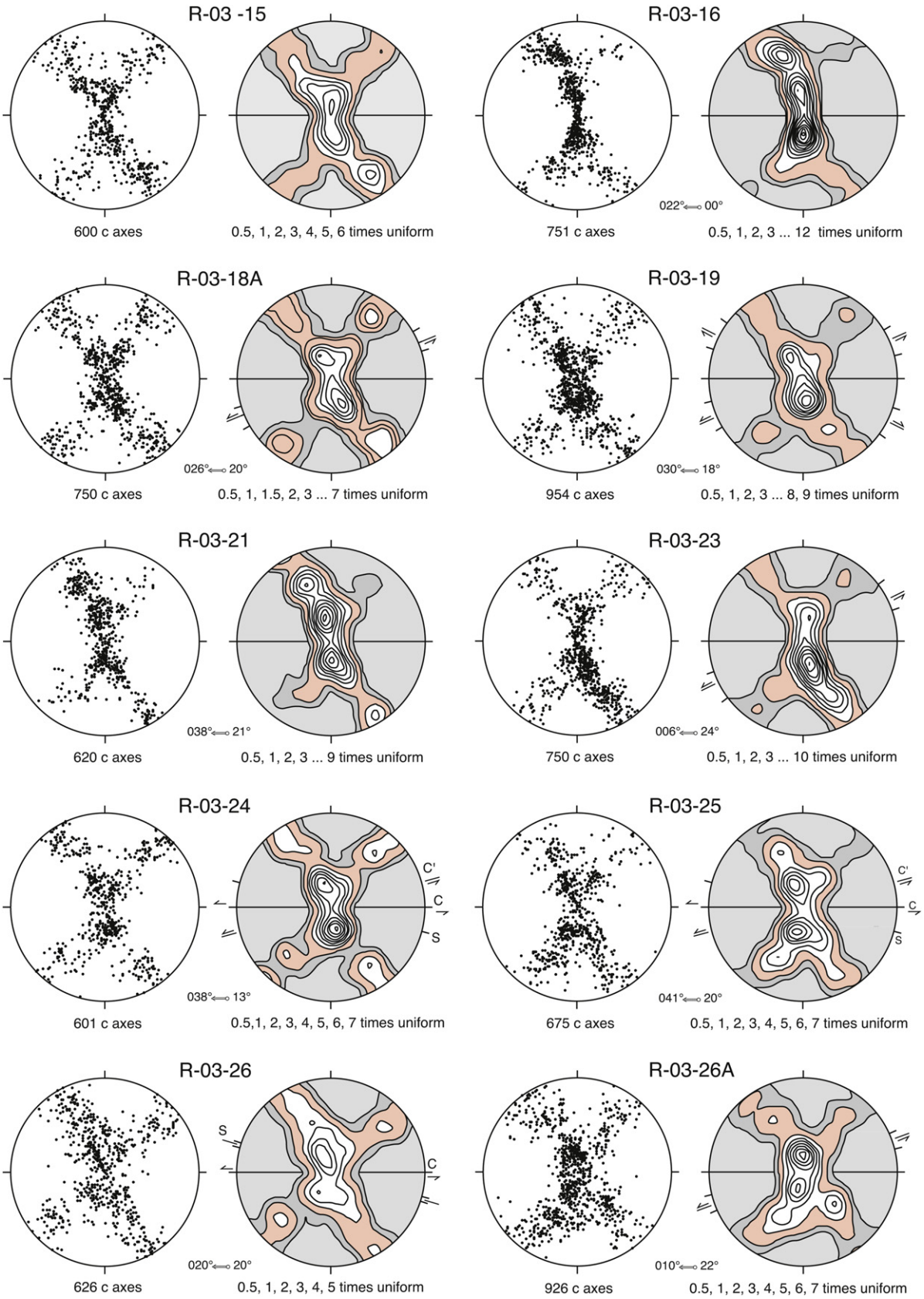

Fig. 9. Optically measured quartz c-axis fabrics for GHS metasedimentary rocks and leucogranite sills (R-03-21, 24, 25 and 26) from the Northern Transect. All lower hemisphere equal area projections viewed towards the east and oriented perpendicular to foliation (horizontal line) and parallel to stretching lineation. Fabrics arranged in order of increasing structural distance beneath detachment (see also Figs. 3 and 10). All *in-situ* oriented samples; plunge and trend of lineation, range of shear band orientations and contour intervals indicated for each sample. Skeletal fabric parameter data for these samples are summarized in Supplementary Fig. 1 and Table 2.

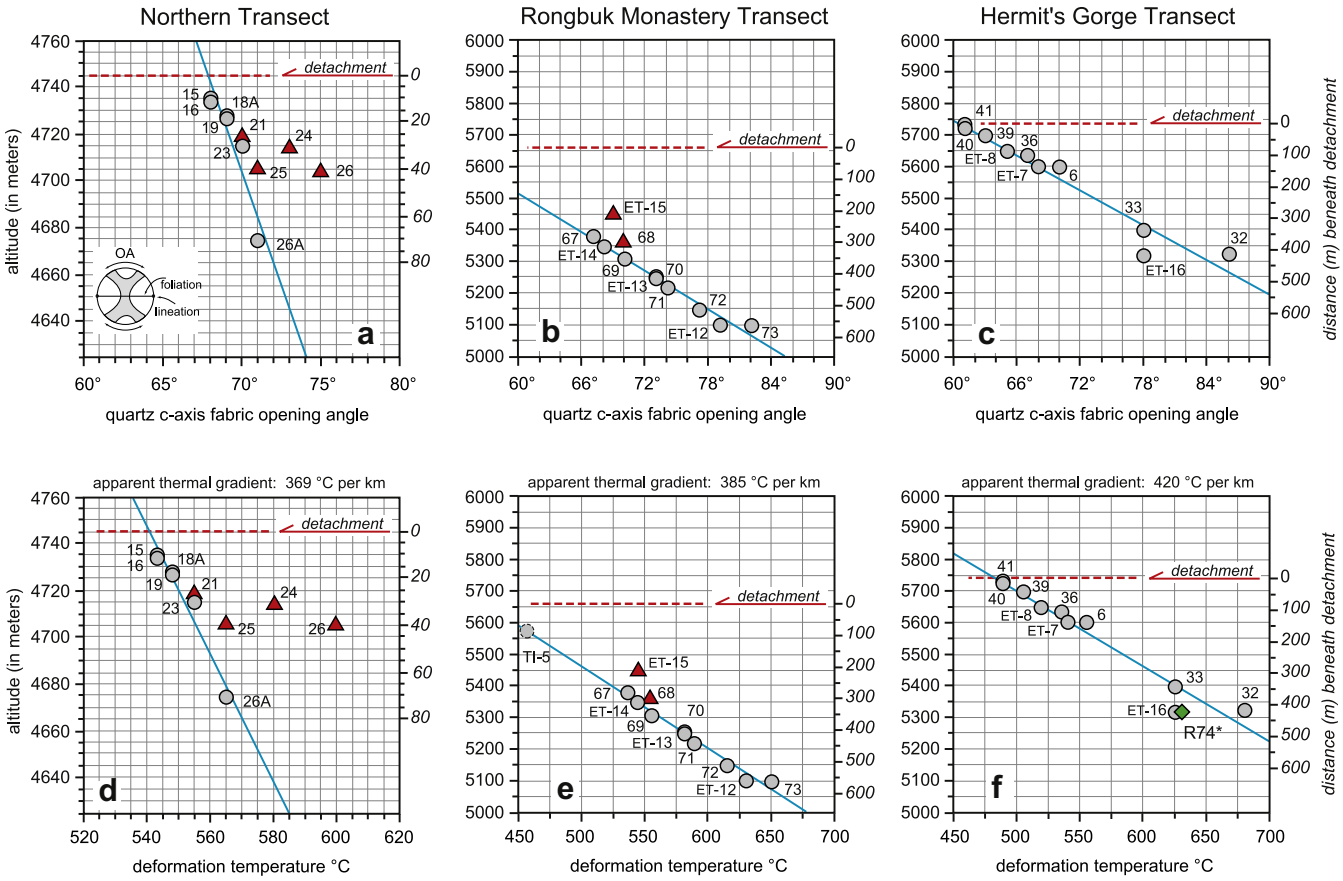

Fig. 10. (a–c) Quartz c-axis fabric opening angle data from the Northern, Rongbuk Monastery and Hermit's Gorge transects. Circles – metasedimentary rocks, triangles – leucogranite sills; linear regression lines through data from metasedimentary rock samples from each transect indicated. Fabric diagrams for the three transects are shown in Figs. 7–9, and skeletal fabric parameter data (including opening angles) are summarized in Supplementary Fig. 1 and Table 2. (d–f) Corresponding deformation temperatures indicated by the Kruhl (1998) opening angle thermometer; details of thermometer are given in Supplementary Fig. 2. Deformation temperatures have a ±50 °C confidence limit; error bars not shown. For Hermit's Gorge Transect (f), note close correspondence between deformation temperature (625 °C) indicated for sample ET-16 and peak metamorphic temperature of 630 °C estimated by Hodges et al. (1992) for sample R74 collected from the same outcrop and based on simultaneous garnet-biotite and garnet-plag-sill-qtz thermobarometer. Positions of samples beneath the gently dipping detachment indicated both by altitudes above sea level and structural distance beneath detachment; see text for further details. Note different vertical scale used for Northern Transect (a, d). See Fig. 3 for sample locations.

rotatation and grain boundary migration of quartz and has a fabric opening angle of 57° (Fig. 8) indicating a deformation temperature of c. 460 °C using the Kruhl (1998) thermometer. Extrapolation of the observed linear relationship between fabric opening angle/deformation temperature and structural position in the quartz-rich metasedimentary rocks on this transect suggest that TI-5 may have been eroded from an outcrop located at c. 75 m beneath the detachment (Fig. 10e). Traced structurally downwards on the Rongbuk Monastery transect, within the more pelitic samples analyzed, sillimanite first appears in sample ET-13; the fabric opening angle in this sample indicates a deformation temperature of c. 580 °C (Fig. 10e). The sillimanite in this sample is drawn into top down to the north shear bands but has suffered only minor retrogression (Law et al., 2004, their Fig. 4e,f). For the samples collected, maximum deformation temperatures of c. 650 °C are reached at a depth of 560 m beneath the detachment on the Rongbuk Monastery transect.

In comparison with the Hermit's Gorge and Rongbuk Monastery transects, the Northern transect is very short, with the majority of samples being collected at depths of less than 30–40 m beneath the detachment. Deformation temperatures of c. 540 °C are indicated by fabric opening angles in quartz-rich calc-silicate horizons located at 10 m beneath the detachment, increasing to c. 565 °C in sample R-03-26A, a biotite schist with rare garnet located at an estimated distance of 70 m beneath the detachment (Fig. 10d). This sample was collected some 100 m to the south of the main transect and its estimated distance beneath the detachment takes in to account the observed 10–15° dip to the NNE on local exposures of the detachment surface.

We emphasize that the exceptionally steep, apparently linear thermal gradients indicated for the three Rongbuk transects (Fig. 10d–f) cannot continue to any great depth in the GHS rocks below the floor of the Rongbuk Valley, but must rapidly decrease traced downwards towards the core of the GHS where peak metamorphic temperatures of c. 700–750 °C are recorded in the Everest region (e.g. Pognante and Benna, 1993; Searle et al., 2003; Cottle et al., 2007, 2009). The mirror image of such a deformation temperature profile has recently been recorded by Law et al. (2011, unpublished data) above the Main Central thrust (MCT) in the Sutlej Valley of the western Himalaya (Fig. 1). Here deformation temperatures of c. 535, 560, 600 and 615 °C are indicated by quartz fabric opening angles in GHS rocks at structural heights of 75, 200, 750 and 1150 m, respectively above the MCT. These data define a power law (rather than linear) relationship between deformation temperature and structural height, with apparent thermal gradients smoothly decreasing up section from c. 175 °C per km at 75–200 m above the MCT to c. 35 °C per km at 750–1150 m above the MCT.

3.5. Deformation temperatures in leucogranites and adjacent metasedimentary rocks

As noted above, fabric opening angles in the plastically deformed leucogranite sills are always larger than in the adjacent metasedimentary rocks (Fig. 10a,b), with greater differences in opening angle being associated with the thicker sills. Using the Kruhl (1998) thermometer, and assuming that "average" deformation temperatures in the surrounding metasedimentary rocks are approximated by the linear regression lines shown in Fig. 10d,e, the opening angle data may be used to estimate likely differences in deformation temperatures between the leucogranites and their surrounding country rocks. For thin (10–20 cm) sills differences in inferred deformation temperatures are negligible (e.g. 4 °C for leucogranite sample R-03-23 from the Northern transect; Fig. 10d). In contrast, fabric opening angles from the centers of thicker sills indicate significantly higher deformation temperatures than their surrounding country rocks (e.g. 16 °C for sample R-03-68 from a 2–3 m thick sill and c. 45 °C for leucogranite samples ET-15 and R-03-26 from 5 to 10 m thick sills, Fig. 10d,e).

Macroscopic foliation (C surfaces) and lineation in the leucogranites and adjacent metasedimentary country rocks are in closely similar orientations, and microstructures and quartz c-axis fabrics in both units always indicate a top down to the north shear sense, suggesting deformation under the same kinematic framework. The negligible difference in deformation temperatures inferred from fabric opening angles in the thin foliation-parallel sills and adjacent country rocks suggests that the thin leucogranite sills cooled to ambient background temperatures before penetrative deformation ceased. In contrast the larger differences in deformation temperatures between the thicker sills and their country rocks suggests that they had not cooled to ambient temperature (c. 525–550 °C; Fig. 10d,e) when plastic deformation of quartz ceased. This in turn may suggest that at least the leucogranite sills studied were intruded during a relatively late stage of top down to the north penetrative deformation associated with exhumation (Law et al., 2004); cf. 550 °C exhumation position on PT path for Everest Series sample ME-14 (Fig. 4).

3.6. 3D analysis of thermal structure in GHS metasedimentary rocks

Based on linear regression lines through deformation temperature data from the three transects, 2D spatial relationships between the inferred isothermal surfaces connecting the three transects are shown schematically in Fig. 11. The isothermal surfaces connecting the Hermit's Gorge and Rongbuk Monastery transects have an apparent dip of c. 2° towards the NNW along a vertical 324-144° striking section line. The isothermal surfaces connecting the Rongbuk Monastery and Northern transects have an

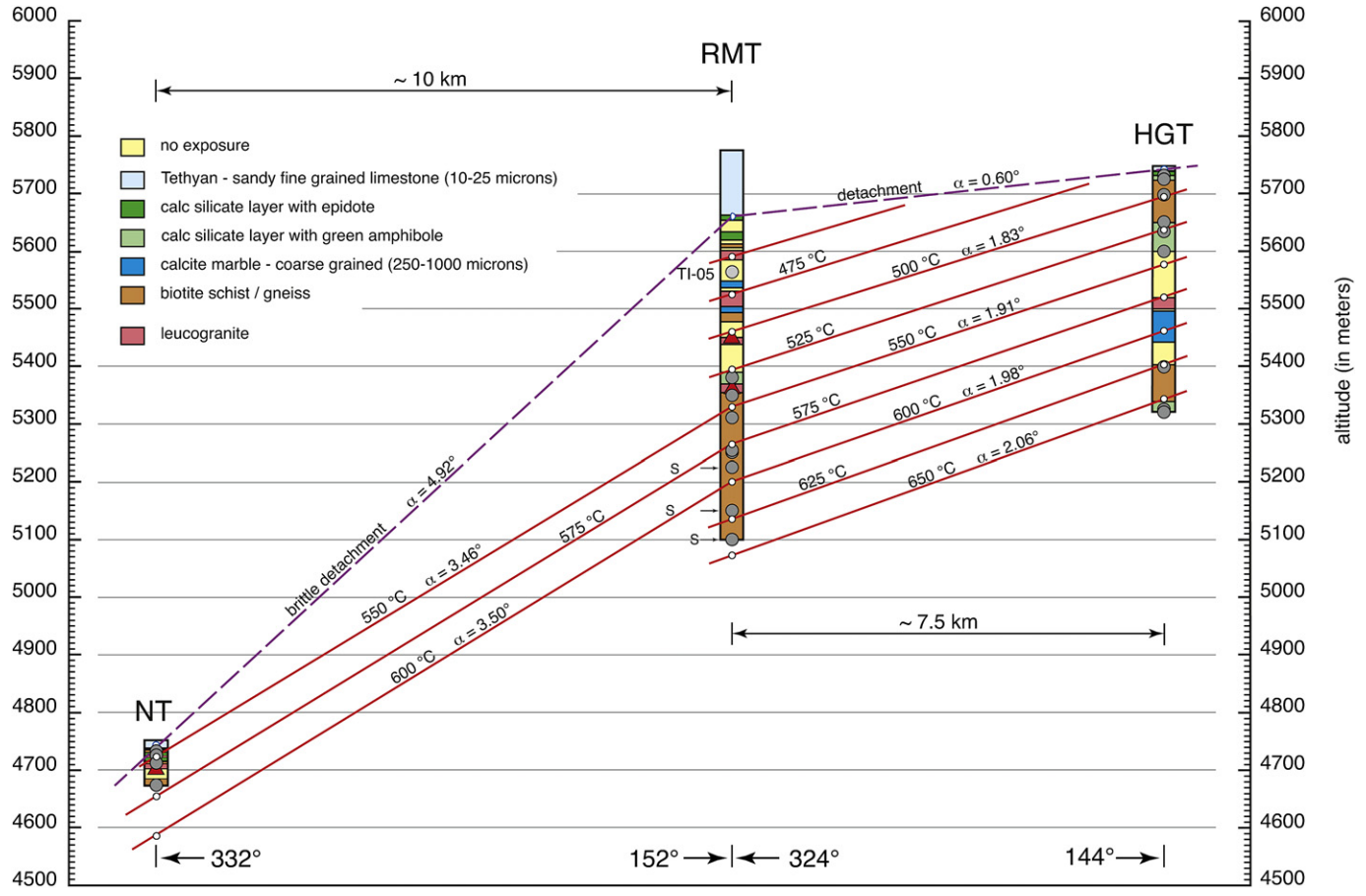

Fig. 11. Correlation of GHS metasedimentary rock deformation temperatures indicated by quartz fabric opening angles (linear regression lines in Fig. 10d–f) in the Northern (NT), Rongbuk Monastery (RMT) and Hermit's Gorge (HT) transects. Apparent dips (α) of isothermal surfaces and detachments in vertical sections drawn between transects are indicated. Strike of the vertical sections between the Northern and Rongbuk Monastery transects, and between the Rongbuk Monastery and Hermit's Gorge transects, are also indicated. Detachment surface between the Rongbuk Monastery and Hermit's Gorge transects corresponds to the combined Lhotse and Qomolangma detachments of Searle (2003); projected detachment surface between the Northern and Rongbuk Monastery transects is probably a later brittle detachment cutting down metamorphic section towards the north. Note: 10:1 exaggeration between vertical and horizontal scales.

apparent dip of c. 3° towards the NNW along a vertical 332-152° striking section line.

The sheet dip of these inferred isothermal surfaces has been estimated by applying a basic *'3 Point Problem'* analysis to the thermal data from the three transects (Fig. 12a). This admittedly crude analysis indicates a strike of c. 135° and a dip of 11° towards the NE for the isothermal surfaces which is very similar to the vector mean orientation of foliation (strike 139°, dip 5° to NE) measured in the three transects (Fig. 5). A similar *'3 Point Problem'* analysis may be applied to the detachment positions in the three transects, once again assuming a simple planar surface. This analysis indicates an 'average' strike of 141° and a dip of 24° towards the NE for the detachment (Fig. 12b), although in reality the three transects may intersect different strands of the STDS and from field observations it is clear that while the detachment (s) is sub-horizontal in the Hermit's Gorge to Rongbuk Monastery area, traced towards the north it progressively dips more steeply, attaining a dip of c. 10–15° towards the NNE on the Northern transect. Nonetheless it is clear that foliation and thermal surfaces in the GHS metasedimentary rocks have a closely similar strike (at least within c. 6°) to the overlying detachment, although the dip (towards the NE) of these three structural features vary slightly (5–10°) with respect to each other. The late brittle detachment mapped between the Rongbuk Monastery and Northern transects (e.g. Burchfiel et al., 1992; Carosi et al., 1998; Fig. 3) cuts down section across the isotherms in the underlying GHS (Fig. 11).

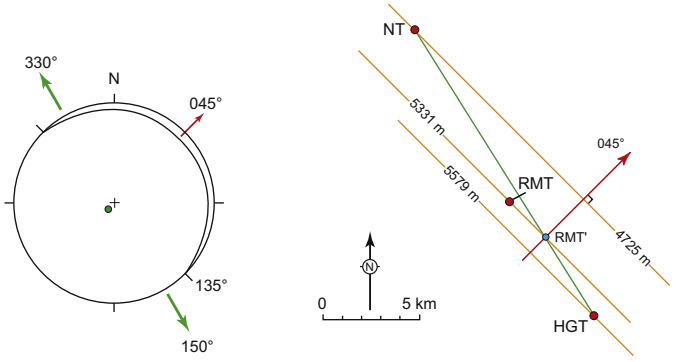

a 3 Point Problem on 550 °C isotherm: strike 135°, dip 11° NE

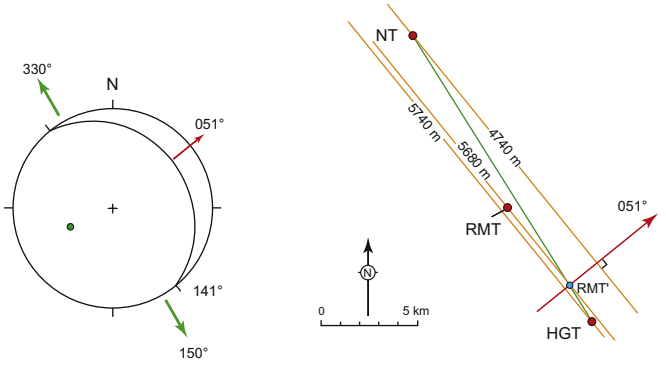

b 3 Point Problem on detachment surface: strike 141°, dip 24° NE

Fig. 12. Strike and dip estimates for 550 °C isothermal surface (a) and detachment surface (b), based on *3 Point Problem* analyses of data summarized in Fig. 11 for the Northern (NT), Rongbuk Monastery (RMT) and Hermit's Gorge (HGT) transects. In both cases the simplifying assumption of a single planar surface is made, while in reality detachment surface(s) between the NT and RMT and between the RMT and HGT are probably of different ages.

3.7. Strain rates in GHS metasedimentary rocks

Strain rates associated with penetrative deformation during exhumation of the Rongbuk metasedimentary rocks (Supplementary Table 1) have been estimated using the quartz flow laws of Hirth et al. (2001) and Rutter and Brodie (2004), based on differential stresses and deformation temperatures indicated by grain size of recrystallized quartz (Section 3.1) and quartz fabric opening angles (Section 3.4), respectively, and using water fugacities appropriate to estimated deformation temperatures and associated pressures for individual samples. Details of these analyses will form the subject of a separate paper. Here we simply highlight the main findings of these analyses and their implications for flow in the footwall to the detachment.

Average differential stress and deformation temperature estimates for the three Rongbuk transects are compiled in Fig. 13a and b, respectively and plotted against distance beneath the detachment. Deformation temperatures estimated from fabric opening angles (and also qualitatively inferred from quartz recrystallization regimes and onset of plasticity in feldspar) progressively decrease traced upwards towards the overlying detachment (Fig. 13b). In contrast, differential stresses estimated from recrystallized quartz grain size remain fairly constant traced upwards towards the detachment (the Stipp and Tullis, 2003 piezometer in this grain size regime is relatively insensitive to large changes in grain size), only increasing in magnitude within 50–75 m of the overlying detachment (Fig. 13a). Both the Hirth et al. (2001) and Rutter and Brodie (2004) flow laws indicate that strain rates progressively decrease traced structurally upwards in to the cooler rocks (Fig. 13c,d), only increasing in the immediate footwall to the detachment where the highest differential stress magnitudes are indicated by the smallest recrystallized grain sizes. In these rocks located immediately beneath the detachment, higher strain rates would be indicated if only flow stresses estimated from small quartz grains dominated by sub-grain rotation recrystallization were used, while lower strain rates would be indicated if only stresses estimated from the larger quartz grains dominated by grain boundary migration recrystallization were used (see Section 3.1). It should be noted that deformation temperatures for these samples are based on quartz fabrics measured on the dominant larger grains in these samples.

Strain rates of 10^{-13} s^{-1} are indicated by the Hirth et al. (2001) flow law for samples located at the greatest distances (>c. 450 m) beneath the detachment (Fig. 13c; Supplementary Table 1). Strain rates estimated using the Hirth et al. (2001) flow law decrease up section to 10^{-14} s^{-1} at ~ 100–150 m beneath the detachment and then increase to 10^{-13}–10^{-12} s^{-1} at < 100 m beneath the detachment. A similar upward change is observed in strain rates indicated by the Rutter and Brodie (2004) flow law (Fig. 13d), although strain rates are slower for individual samples than strain rates indicated by the Hirth et al. (2001) flow law. Strain rates based on the Rutter and Brodie (2004) flow law (Fig. 13d) are approximately an order of magnitude slower at >450 m beneath the detachment. This difference in estimated strain rates based on the two flow laws increases traced up section towards the detachment. The observed non-linear relationship between strain rates indicated by the two flow laws for the Rongbuk samples is due to the different sensitivities of the flow laws to changing conditions of flow stress and deformation temperature (Fig. 13e,f).

Although both flow laws indicate that the highest strain rates are in the immediate footwall to the detachment, this does not necessarily mean that the highest strain magnitudes are also recorded in these rocks. For example, as noted above, inclusion of grain size data associated with sub-grain rotation recrystallization results in higher flow stresses and faster estimated strain rates than would be obtained solely using the larger grains that developed by

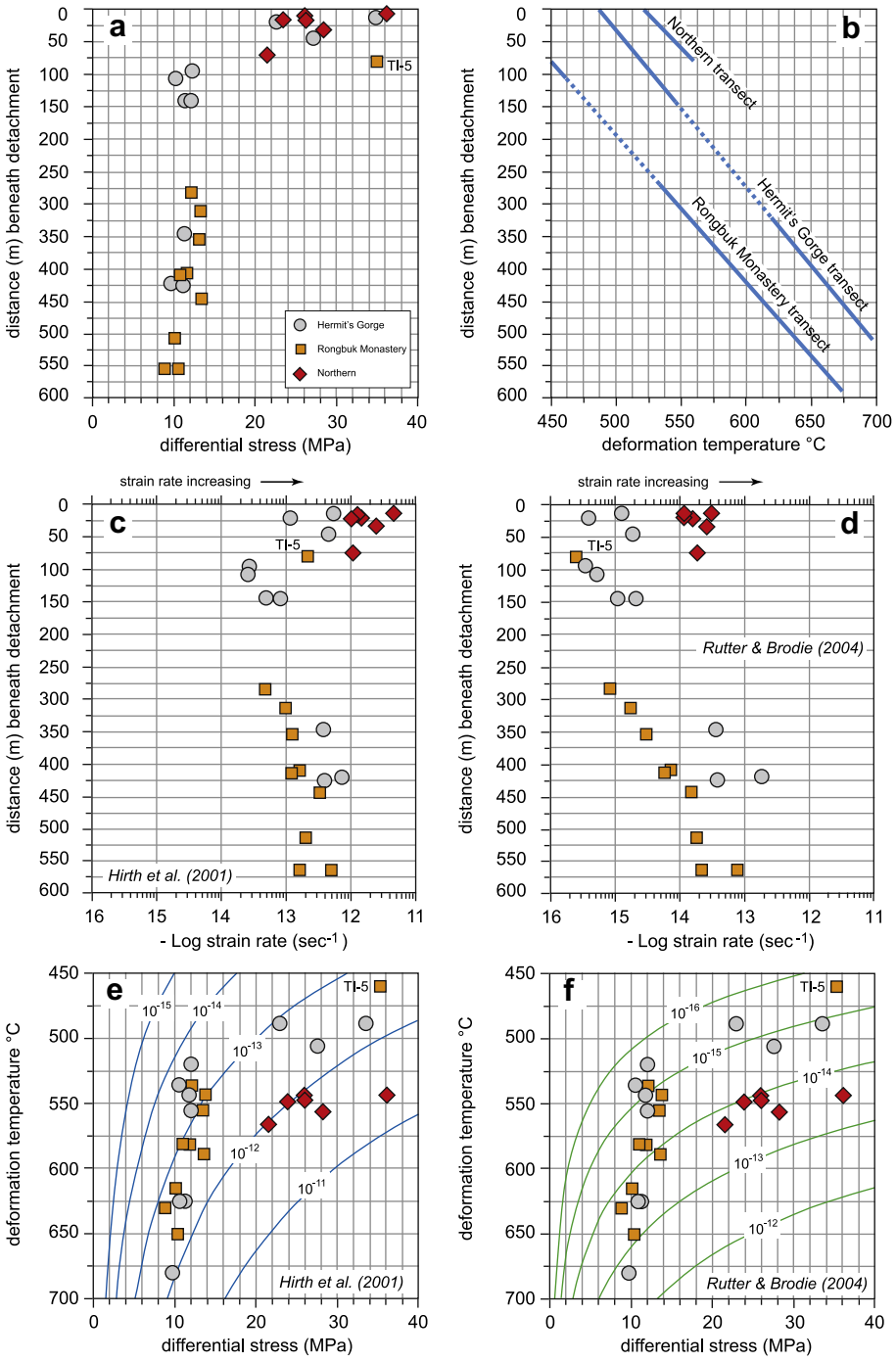

Fig. 13. Compilation of differential flow stress (a), deformation temperature (b) and strain rate data (c–f) for metasedimentary rocks on the Hermit's Gorge, Rongbuk Monastery and Northern transects. (a) Variation in differential stress with depth beneath detachment estimated from recrystallized quartz grain size data using piezometer of Stipp and Tullis (2003) with corrections to original piezometer recommended by Holyoke and Kronenberg (2010); data compiled from Fig. 6d–f. Structural position of sample TI-5 on the Rongbuk Monastery transect is inferred from its fabric opening angle and where this would fall on linear regression line of structural position versus opening angle for *in-situ* samples on this transect (Fig. 10e). (b) Deformation temperatures indicated by the Kruhl (1998) quartz c-axis fabric opening angle thermometer; linear regression lines through data in Fig. 10d–f shown; dashed lines indicate parts of transects dominated by marble and calc-silicate horizons; cf. Fig. 11. (c,d) Variation in estimated strain rates with distance beneath detachment using quartz flow laws of Hirth et al. (2001) and Rutter and Brodie (2004) with differential stress and deformation temperature data from recrystallized grain sizes (a) and fabric opening angles (b), respectively; note that strain rate increases towards the right in each diagram. Quartz flow law parameters used are as published (Hirth et al., 2001; Rutter and Brodie, 2004) with the exception of the water fugacity term, which has been modified for estimated PT conditions under which quartz fabrics (Figs. 7–10d–f) formed in individual samples. (e,f) Relationships between estimated deformation temperatures/differential flow stresses for samples from the three Rongbuk transects and strain rates indicated by the water fugacity-normalized quartz flow laws of Hirth et al. (2001) and Rutter and Brodie (2004).

grain boundary migration recrystallization. We remain uncertain if these small equant recrystallized grains developed synchronously with, or possibly after, grain boundary migration recrystallization that dominates the Rongbuk transects. Additionally, Jessup et al. (2006) have shown that the vorticity of flow increases traced structurally upwards in all three of the Rongbuk transects. Variation in strain path (pure, general or simple shear) is not explicitly factored in to these flow laws and strain rate calculations. As strain

magnitudes increase more slowly in simple shear than in pure shear (Pfiffner and Ramsay, 1982) then, for a given number of strain increments, lower finite strain magnitudes would be expected in the simple shear-dominated (and cooler) rocks adjacent to the detachment, while higher strain magnitudes would be expected in the pure shear dominated (and hotter) rocks at greater distances beneath the detachment.

3.8. Caveats for using microstructures and crystal fabrics as deformation thermometers

Within our GHS samples a close agreement is observed between deformation temperatures indicated by microstructures (e.g. quartz recrystallization regimes, onset of plasticity in feldspar) and quartz c-axis fabric opening angles. It must be emphasized, however, that these microstructure- and fabric-based thermometers (e.g. Kruhl, 1998; Stipp et al., 2002a) assume 'average' geologic strain rates. In general, microstructures and crystal fabrics develop in response to a complex inter-play of different extrinsic and intrinsic factors. For example, from experimental and numerical modeling studies (e.g. Tullis et al., 1973; Lister and Hobbs, 1980; Lister and Dornsiepen, 1982) it is known that quartz c-axis fabric opening angles increase with increasing deformation temperature and hydrolytic weakening and decreasing strain rate. Use of quartz c-axis fabric opening angles as a deformation thermometer (Supplementary Fig. 2) assumes that deformation temperature is the prime control on fabric opening angle. Similarly, quartz recrystallization mechanisms such as grain boundary bulging, subgrain rotation and grain boundary migration, have also been demonstrated experimentally to be controlled by deformation temperature, hydrolytic weakening and strain rate. Once again, use of these microstructures as deformation thermometers assumes that deformation temperature is the prime controlling factor and that deformation has occurred at *'average geological strain rates'*.

In the case of our Rongbuk samples it could be argued that the observed decrease in fabric opening angles traced structurally upwards towards the overlying detachment (Fig. 10a–c) is a reflection of increasing strain rates rather than decreasing deformation temperatures. A similar strain rate interpretation could be placed on the observed transitions in quartz recrystallization regimes and feldspar rheology traced towards the detachment. In contrast, our integrated piezometry and deformation temperature data suggest that strain rates decrease slightly traced up section towards the detachment in to cooler rocks, only increasing within c. 50 m of the detachment (Fig. 13c,d). However, because these estimated strain rates are partially based on deformation temperatures inferred from fabric opening angles, they cannot, of course, be used as an independent indicator of the validity of using fabric opening angles as a deformation thermometer.

Alternatively it could be argued that the observed spatial transitions in microstructures and fabric opening angles are a reflection of increased hydrolytic weakening traced away from the detachment surface, although intuitively we would expect fluid flux and hydrolytic weakening to be focused close to the detachment. Nonetheless the larger opening angles observed in the leucogranite sills, relative to the surrounding metasedimentary rocks, could be explained by the focusing of fluids and hydrolytic weakening in these syn-kinematic intrusions. Although beyond the scope of our current study, clearly what is needed here is a thermometer that is independent of variables such as strain rate and hydrolytic weakening.

One such study across the STDS has recently been described from the Dzakaa Chu valley, located 50 km to the WNW of the Hermit's Gorge transect (Fig. 1). Here the STDS is marked by a ~1 km thick shear zone dipping at c. 30° N and separating Tethyan limestones from underlying ampibolite facies GHS rocks (Cottle et al., 2007). Metamorphic conditions in this shear zone were assessed by Cottle et al. (2011) using both Raman spectroscopy on carbonaceous material (RSCM) and phase equilibria modeling. Both thermometry methods are independent of strain rate and hydrolytic weakening, and RSCM data are regarded as providing estimates of maximum temperatures attained during burial and therefore prior to exhumation. Results from these thermometers are in agreement at the upper and lower boundaries of the shear zone, but within the shear zone RSCM temperatures were consistently higher (by up to 100 °C) than metamorphic temperatures indicted by petrologic indicators and deformation temperatures indicated by quartz and calcite microstructures. Cottle et al. (2011) estimated peak metamorphic temperatures in the hanging wall limestones of ~340 °C. These peak temperatures increased down structural section to ~650 °C at the base of the shear zone, defining an average metamorphic field gradient of ~310 °C per km across the entire shear zone.

We regard the similar apparent thermal gradients across the STDS on the Dzakaa Chu (310 °C per km) and Rongbuk transects (369, 385 and 420 °C per km traced from the Northern transect southwards through the Rongbuk Monastery to the Hermit's Gorge transect) as providing strong supporting evidence that measured fabric opening angles from the Rongbuk transects are primarily controlled by deformation temperature. Although beyond the scope of our current project, we would nonetheless argue that more direct independent assessments of deformation temperatures for the Rongbuk transects should be made where possible. The recently proposed titanium in quartz thermometer (Wark and Watson, 2006) incorporating appropriate corrections for pressure and titanium activity (Thomas et al., 2010) may be a useful technique for independently assessing deformation temperatures for the Rongbuk samples. Although debate continues over minimum temperatures at which the technique is likely to give meaningful results (cf. Kohn and Northrup, 2009; Grujic et al., 2009), the majority of the Rongbuk samples have clearly been exhumed under amphibolite facies conditions (>500 °C) where grain boundary migration should promote the equilibration of Ti in quartz (Grujic et al., 2009, 2011) and therefore the technique should provide information on deformation temperatures prevailing during exhumation-related fabric development. Similarly, infrared spectroscopy (Kronenberg and Wolf, 1990) could be employed to determine intragranular water content in the quartz-bearing rocks and hence investigate the likely role of hydrolytic weakening in controlling recrystallization mechanisms and fabric opening angles.

4. Telescoping of isotherms

Telescoping of isotherms in the footwall to the STDS could be due to a number of tectonic processes either acting singly or in tandem with each other. Below we discuss three of the most commonly cited groups of processes for telescoping of isotherms/isograds (penetrative pure shear vertical shortening, heterogeneous simple shear, general shear) and their implications for transport magnitudes associated with exhumation of these footwall rocks.

4.1. Penetrative pure shear vertical shortening

The observed telescoping of isotherms on the Rongbuk transects (Figs. 10 and 11) could be explained by penetrative vertical shortening due to lithostatic loading. A highly simplified scenario of a pure shear deformation (plane strain at constant volume) involving vertical principal shortening and horizontal 475 and

675 °C isotherms is shown in Fig. 14 for assumed initial geothermal gradients of 25 and 40 °C per km. The 475 and 675 °C isotherms were chosen to represent the lower and upper bounds of deformation temperatures indicated by fabric opening angles on the Rongbuk transects. The vertical separation between these isotherms on the transects is c. 0.5 km (Fig. 10e,f).

For an initial geothermal gradient of 25 °C per km a vertical shortening of 93.75% shortening would be needed to condense (or telescope) the 475 and 675 °C isotherms from an original vertical separation of 8.0 km to a final separation of 0.5 km (Fig. 14a). Similarly, for an initial geothermal gradient of 40 °C per km a vertical shortening of 90% shortening would be needed to telescope the 475 and 675 °C isotherms from an original vertical separation of 5.0 km to a final separation of 0.5 km (Fig. 14b). These shortening strains could accumulate in ~0.3–3.0 Myr at the strain rates of 10^{-13}–10^{-14} s^{-1} indicated by our differential stress and deformation temperature data (Fig. 13c). Assuming plane strain constant volume deformation. the 93.75 and 90% vertical shortening estimates would correspond to horizontal stretches of 1500% ($1 + e_1 = 16$) and 900% ($1 + e_1 = 10$) respectively, and Rxz strain ratios of 256:1 and 100:1 respectively. These exceptionally large magnitude stretches present obvious space problems, even assuming that exhumation is ultimately driven by transport-parallel flow (Fig. 2).

Clearly at such extreme finite strain magnitudes, the Rongbuk transects should be characterized by pervasive development of mylonite-ultramylonite. However, although discreet foliation-subparallel mylonitic shear zones are locally observed, the bulk of the transects are composed of schists and gneisses lacking any textural evidence for such intense penetrative straining. Law et al. (2004) estimated Rxz strain ratios of 2.05–2.75 based on the aspect ratios of dynamically recrystallized quartz aggregates that are enveloped by mica films, in reconnaissance samples collected from the Hermit's Gorge and Rongbuk Monastery transects. These are undoubtedly minimum Rxz strain estimates. However, as indicated in Supplementary Fig. 3 (Wallis (1992, 1995)), β angles measured between foliation and the central segment of the cross-girdle quartz c-axis fabrics in these reconnaissance samples indicate maximum possible Rxz strain ratios of between c. 5:1 and 18:1, assuming that deformation has a vorticity number (Wm) less than or equal to 1 (i.e. simple shear or a general shear involving a combination of simple and pure shear). Based on several methods of vorticity analysis, Law et al. (2004) and Jessup et al. (2006) have previously estimated Wm values of 0.57–0.94 (c. 62-20% pure shear) for GHS samples collected along the three transects, with Wm values increasing structurally upwards towards the overlying detachment. Integrated vorticity and Rxz strain ratios (albeit minimum strain values) indicated shortening estimates of c. 10–30% with associated transport-parallel stretches of c. 10–40% (Law et al., 2004, their Fig. 15). Thus, while estimates of vertical (pure shear) shortening required to explain telescoping of the isotherms are too high to be compatible with textural and crystal fabric data, the two orders of magnitude lower shortening estimates indicated by integrated strain and vorticity analyses are too low to explain (at least by themselves) the extreme telescoping of the isotherms.

4.2. Heterogeneous simple shear during exhumation

Telescoping of isotherms in the Rongbuk transects could be due to differential transport-parallel motion between samples in the footwall to the detachment. This scenario is illustrated in Fig. 15a where two footwall particles (S1 and S2 originally at 625 and 525 °C, respectively) move along different paths parallel to the overlying detachment during extrusion/exhumation, with the sample in the deeper and hotter part of the footwall moving a greater distance in a given time interval. The assumed particle paths are very similar to those predicted by Grujic et al. (2002) for channel flow with displacement magnitudes increasing inwards from the walls of the channel to the high temperature core (Fig. 2d).

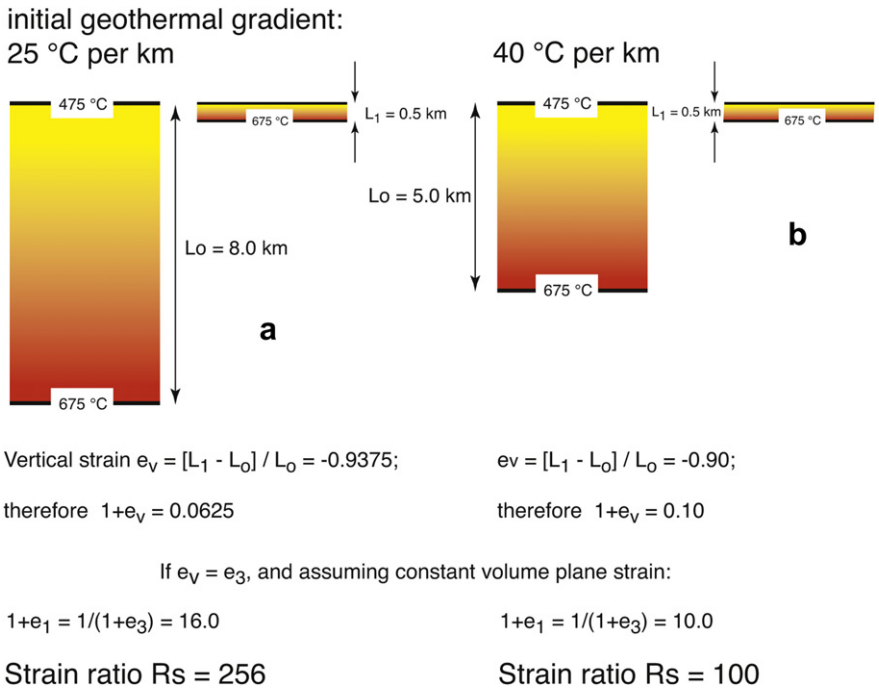

Fig. 14. Pure shear model of shortening required to reduce vertical spacing between 475 and 675 °C isotherms to 500 m, as observed on Rongbuk Monastery and Hermit's Gorge transects (Fig. 10e,f) for initial geothermal gradients of 25 °C per km (a) and 40 °C per km (b). Resultant stretches ($1 + e_1$) perpendicular to shortening assume constant volume plane strain deformation.

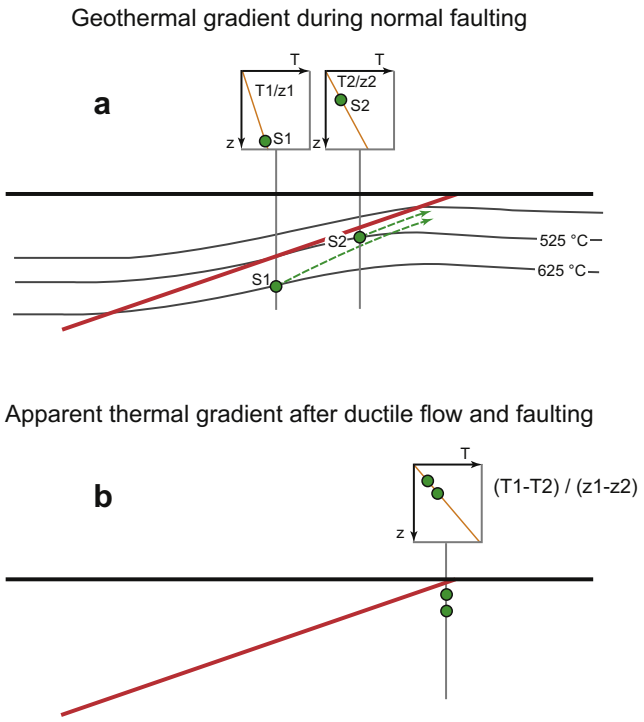

Fig. 15. Particle path model for exhumation in footwall to detachment, with displacement of particles parallel to overlying detachment surface progressively increasing downwards away from detachment – as predicted for channel flow (Fig. 2d). (a) Original positions of two particles S1 and S2 at 525 and 625 °C, respectively, with large component of vertical separation; *'normal'* geothermal gradient. (b) After displacement vertical component of separation between particles S1 and S2 is reduced, resulting in steeper apparent thermal gradient between the two particles. Diagram courtesy of Bernhard Grasemann, 2004.

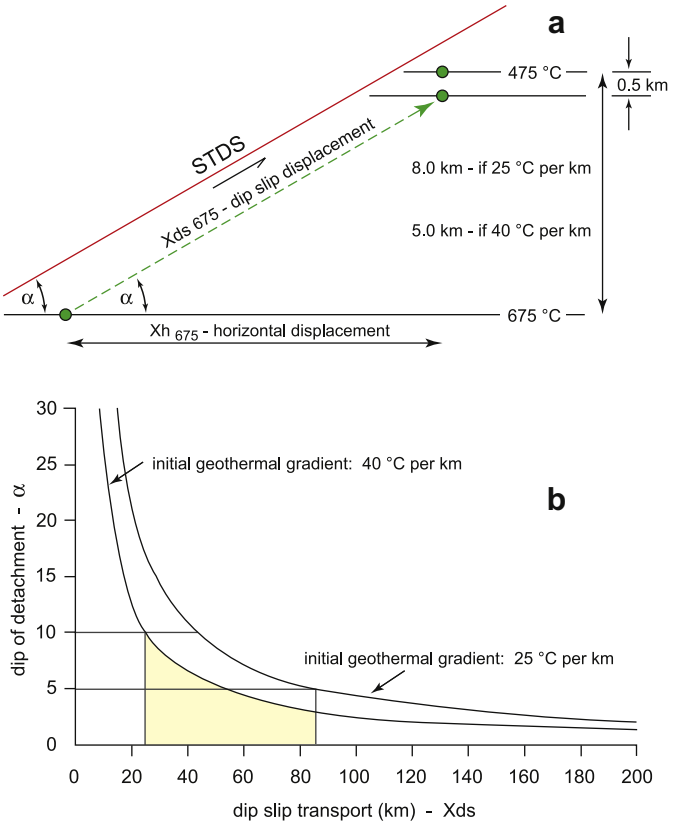

Fig. 16. Particle Displacement Model 1. 475 °C particle remains in a fixed position while 675 °C particle moves upwards along a path parallel to the overlying detachment (STDS) reducing the vertical component of separation between the two particles. Dip of detachment – α. 475 and 675 °C isothermal surfaces assumed to be horizontal and inclined at angle α to detachment. Penetrative strain not considered in this model.

In its most basic form the particle path model can be thought of as a heterogeneous simple shear model in which the flow plane is oriented parallel to the overlying detachment surface. Although no penetrative shortening occurs measured perpendicular to the flow plane (assuming strict simple shear) particles S1 and S2 which were originally widely separated in the vertical direction (Fig. 15a) are now considerably closer together (Fig. 15b). Assuming that the original metamorphic mineral assemblages/microstructures/crystallographic fabrics in particles S1 and S2 are not overprinted by lower temperature features during or after movement along their respective exhumation paths, then telescoping of the isotherms indicated by these thermometers is produced, resulting in steeper apparent thermal gradients (Fig. 15b).

Based solely on the geometric features of the particle path model we have investigated the likely magnitudes of particle flow, measured parallel to the dip direction of the detachment, that would be consistent with the observed telescoping of isotherms on the Rongbuk transects (Figs. 16 and 17). Geometric variables in this simple 2D analysis include: 1) the dip angle (α) of the detachment and, 2) the original vertical spacing between isotherms – for which we assume prevailing linear geothermal gradient of 25 or 40 °C per km. We also assume that isotherms were originally horizontal and therefore inclined to the detachment surface at an angle equal to the detachment dip (α). If the isograds were originally dipping towards either the hinterland or foreland this would decrease or increase, respectively, the angle (α′) between the detachment and the isotherms.

In our first model (Fig. 16a) we assume that a reference particle at 475 °C remains stationary while a particle at 675 °C moves upwards parallel to the overlying detachment until it reaches a vertical distance of 0.5 km below the 475 °C reference particle. For detachment dip angles of 10-5°, as observed between the Hermit's Gorge and Northern transects, dip-slip displacements of c. 44–85 km are indicated for the 675 °C particle assuming a 25 °C per km geothermal gradient, while displacements of c. 25–45 km are indicated assuming a 40 °C per km geothermal gradient (Fig. 14b). For these very low (5–10°) detachment dip angles there is a negligible difference between the dip slip and horizontal components of displacement. These displacement estimates for individual particles are presumably minimum estimates because the quartz c-axis fabrics and related opening angles used to estimate deformation temperatures are themselves the products of the exhumation-related shearing and cooling, with the recorded fabrics for individual particles (Figs. 7–9) being 'locked in' at a particular deformation temperature during exhumation. In this scenario higher temperature fabrics that developed during the structurally deeper and earlier stages of exhumation would have been progressively overprinted by lower temperature fabrics during exhumation-related cooling. However, fabrics and microstructures in both the footwall and hanging wall to the STDS (Rongbuk and Dzakaa Chu transects; Everest Series samples from above East Rongbuk Glacier and on Everest NE Ridge, Waters unpublished data) appear to have been locked in before deformation temperatures experienced by individual particles had significantly fallen from the pre-exhumation peak. This is particularly evident in the Dzakaa Chu section across the STDS (Fig. 1; see Section 3.8) where there is a close correspondence (within 50 °C) between deformation temperatures indicated by microstructures and peak temperatures indicated by Raman spectroscopy on carbonaceous material (Cottle et al., 2011; their Fig. 8).

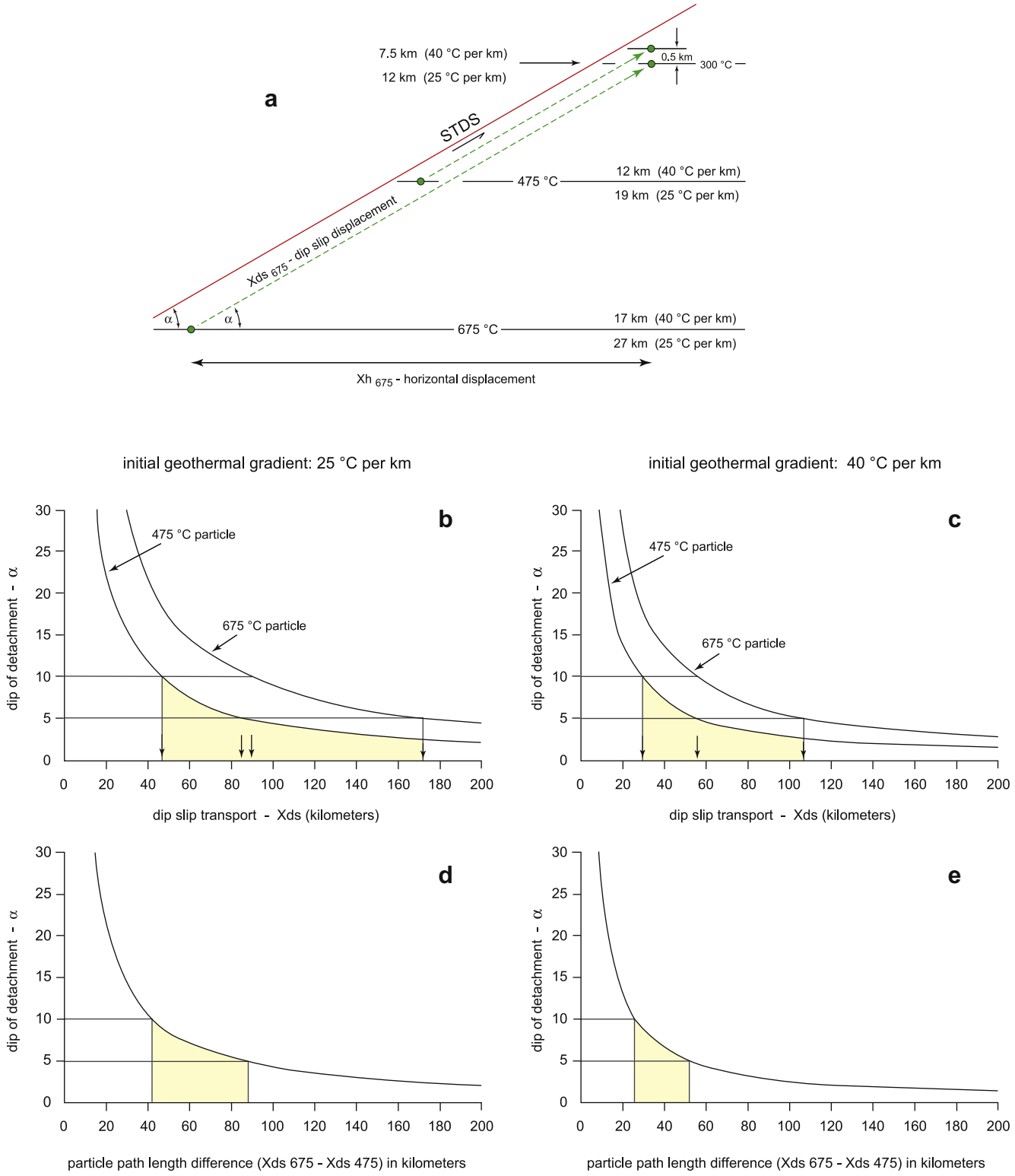

Fig. 17. Particle Displacement Model 2. Both 475 and 675 °C particles move upwards along paths parallel to the overlying detachment (STDS), but 675 °C particle in hotter lower viscosity part of the shear zone/channel moves upwards at a greater velocity (cf. Fig. 2d) thereby reducing the vertical component of separation between the two particles. 475 and 675 °C particles are assumed to become coupled at a vertical separation of 0.5 km as they enter the brittle-ductile transition zone (assumed ambient temperature of c. 300 °C). Penetrative strain not considered in this model.

In our second model (Fig. 17a) we assume that both the 475 and 675 °C particles move upwards parallel to the overlying detachment, and that the particles move independently of each other until they enter the brittle-ductile transition zone (c. 300 °C) where they become coupled at a vertical distance of 0.5 km from each other. For an initial geothermal gradient of 25 °C per km and detachments dips of 10-5°, dip-slip displacement of 86–170 km are indicated for the 675 °C particle, while displacements of 44–86 km are indicated

for the 475 °C particle (Fig. 17b). In contrast, for an initial geothermal gradient of 40 °C per km and detachments dips of 10-5°, dip-slip displacement of 54–108 km are indicated for the 675 °C particle, while displacements of 28–55 km are indicated for the 475 °C particle (Fig. 17c). Differential movement between such reference particles is the primary feature of our second model and is also predicted by channel flow models in which the magnitude of particle displacement increases inwards from the walls towards the high temperature core of the channel (Fig. 2d). For an initial geothermal gradient of 25 °C per km and detachments dips of 10–5°, path length differences of 42–84 km are estimated between the 675 and 475 °C particles (Fig. 17d), while path length differences of 26–54 km are estimated for a geothermal gradient of 40 °C per km (Fig. 17e).

In summary, our two particle path models suggest that detachment-parallel transport magnitudes of c. 25–170 km are needed to explain the observed telescoping of isotherms on the Rongbuk transects. Using similar particle path models Cottle et al. (2007, 2011) have previously estimated detachment-parallel transport magnitudes of ~60 km for the Dzakaa Chu section across the STDS (Fig. 1) using both thermometry and barometry data. Although subject to a wide degree of uncertainty, these transport magnitudes are at least compatible with, and probably conservative compared to, transport magnitudes associated with channel flow models for extrusion/exhumation of the GHS (e.g. Beaumont et al., 2001, 2004). However, these displacement estimates are more difficult to reconcile with recently proposed tectonic models (e.g. Robinson et al., 2006; Yin, 2006, p. 26, 88, 108; cf. Kohn, 2008, p 270) in which the GHS was transported southwards on underlying thrusts with the STDS acting as roof fault and playing only a minor role in extrusion/exhumation of the GHS.

4.3. Heterogeneous general shear during exhumation

Our particle models discussed above essentially assume heterogeneous simple shear in the GHS, with particles moving parallel to the overlying detachment surface. However, as discussed in Section 4.1 above, vorticity analyses indicate that exhumation-related penetrative deformation of these footwall rocks involves a general shear (Law et al., 2004; Jessup et al., 2006). Integrated vorticity and Rxz strain data (albeit minimum strain values) indicated shortening estimates of c. 10–30% measured perpendicular to the flow plane (assumed to be parallel to the overlying detachment surface) with associated transport-parallel stretches of c. 10–40% (Law et al., 2004). The shortening component of this general shear would reduce both the original angle between the detachment and isotherms and the vertical spacing between the original isotherms (Fig. 16a and Fig. 17a), although not by a sufficient amount to explain the observed telescoping of the isotherms (90–93% shortening; Figs. 10 and 14). Simultaneously, however, the transport-parallel stretching produced by this shortening would contribute to the shear plane-parallel displacements, thereby lengthening the particle path. For example, assuming plane strain constant volume deformation, a 20% shortening perpendicular to the flow plane would be accompanied by a 25% transport-parallel stretch to conserve cross section area (see graphed relationships in Law, 2010, p. 595); i.e. there would be a 25% increase in the particle path lengths indicated in our models (Fig. 16a and Fig. 17a). Estimated vorticity values in the GHS rocks decrease (i.e. pure shear component increases) traced down section away from the detachment surface (Jessup et al., 2006), and therefore the component of transport-parallel stretching would increase traced down section in to the footwall rocks, as assumed in our second model (Fig. 17a) and also predicted by Grujic et al. (2002) for channel flow models (Fig. 2d).

4.4. Comparison with barometry-based models for the Everest Region

We emphasize that in the purely geometric models discussed above, no account is taken of thermal process such as chilling of footwall rocks against cooler hanging wall rocks or thermal relaxation across the shear zone (e.g. Grasemann and Mancktelow, 1993). Nonetheless our displacement estimates based on simple geometric modeling of isotherms are at least similar in magnitude to the exhumation-related displacement estimates by Searle et al. (2002, 2003, 2006) based on barometry data from metamorphic mineral assemblages in GHS rocks located at c. 1.5–2.0 km beneath the Lhotse detachment on the Nepal side of the Mount Everest Massif. Three samples from this locality yield peak metamorphic conditions of c. 620 °C and 4.0–4.9 kbars, corresponding to depths of 14–18 kms for a pressure gradient of 0.285 kbar per km (Searle et al., 2006, p. 358). Assuming a dip of 10° for the STDS north of Rongbuk and a pressure gradient of 0.285 kbar per km, Searle et al. (2006) obtained displacement estimates of c. 90–108 km to bring these rocks to the present day topographic surface on a particle path oriented parallel to the dip of the overlying detachment surface. For a 5° dip on the detachment surface, Searle et al. (2006) obtained corresponding displacement estimates of c. 180–216 km. Our samples from the immediate footwall of the STDS on the Rongbuk transects are not suitable for obtaining pressure estimates, although the garnet bearing sample (R74) described by Hodges et al. (1992) from near the bottom of the Hermit's Gorge transect (Fig. 10f) gives an almost identical PT result of 630 °C and 4.6 kbar (16–17 km), suggesting a similar displacement magnitude based on barometry.

It should be noted that the barometry-based displacement estimates of Searle et al. (2006) relate to exhumation from peak metamorphic conditions to the topographic surface (taken as the 5 km above sea level average elevation of the Tibetan Plateau), and are independent of the thermal structure prevailing during exhumation, with displacement estimates only being influenced by the detachment dip. In contrast, our displacement estimates for models attempting to explain the telescoping of isotherms are only related to part of the total exhumation path and, in addition to having to take in to account the detachment dip, are highly sensitive to variations in the assumed thermal structure during exhumation. Nonetheless, displacement estimates for the 675 °C particle in our models (25–85 km in the first model; 54–170 km in the second model) are at least of the same order of magnitude as the barometry-based estimates (c. 90–216 km) which used samples exhumed from peak metamorphic conditions of c. 620 °C and 4.0–4.9 kbars. Specifically comparing our second model with the barometry-based model of Searle et al. (2006), we note that a displacement of 54–170 km is required to bring our 675 °C particle up to the inferred brittle-ductile transition located at the 300 °C model isotherm. Displacements of 25–120 km are needed to bring the 4.0 and 4.9 kbar samples of Searle et al. (2006) from peak metamorphic conditions up to the same inferred structural level assuming the same 10-5° dip on the detachment and a linear geothermal gradient of between 40 and 25 °C per km.

4.5. Flow process associated with exhumation and telescoping of isotherms

We envisage the exhumation-related flow in the GHS rocks exposed in the Rongbuk transects as involving shear along individual structural planes (e.g. foliation, shear zones) oriented subparallel to the overlying detachment surface, accompanied by general shear flow (shortening perpendicular to the flow plane plus simultaneous transport-parallel stretching) in the rocks between

these discontinuities. Analogous models for strain path partitioning in bulk simple shear systems have previously been proposed by Lister and Williams (1979, their Fig. 14) and Williams et al. (2006, their Fig. 2). These models carry the implication that strain and vorticity estimates based on microstructures and crystal fabrics preserved in individual rock samples only record a fraction of the deformation history accumulating at the scale of the shear zone. However, information on the relative displacement between individual samples/particles, as we have attempted to estimate based on deformation temperatures recorded in samples from the Rongbuk transects, provides a more complete picture of deformation occurring at the larger scale.

We have little direct information on the relative timing for when different high – low temperature microstructures and crystal fabrics observed in the Rongbuk transects were 'frozen' in to our samples during exhumation, or for when exhumation-related deformation commenced in individual samples. For example, was: 1) penetrative deformation simultaneously active throughout the shear zone with hotter, originally deeper, rocks being carried passively up section to be juxtaposed against cooler already deformed overlying rocks or; 2) during their passage to shallower crustal level were these hotter rocks progressively overprinted along their upper boundary by lower temperature fabrics as they came in to contact with cooler overlying hanging wall rocks or; 3) did the locus of pervasive shearing (i.e. upper margin of the zone of channelized flow in the GHS; Fig. 2d) progressively migrate up section in to cooler overlying rocks during progressive exhumation. The third scenario implies an upward widening of the shear zone (*sensu* Type I shear zone of Means, 1995) traced up dip to shallower crustal levels, and would require the underlying originally hotter rocks to be carried passively to shallower crustal levels with 'frozen-in' microstructures/fabrics. In contrast, exhumation of material along an upward narrowing crustal scale shear zone (*sensu* Sibson, 1977, his Fig. 8) would perhaps imply a more pervasive overprinting of high temperature by lower temperature/faster strain rate microstructures/fabrics.

In the Rongbuk samples we have found remarkably little evidence for overprinting of high temperature by lower temperature microstructures and mineral assemblages, as would be expected for scenarios 1 and 2. In both the Rongbuk and Dzakaa Chu transects, and in the Everest Series rocks collected by L.R. Wager in 1933 (see Section 2.1), mineral assemblages defining shear bands reflect a metamorphic grade very similar to peak assemblages in the matrix. In addition, mineral assemblages in extensional vein sets that post-date ductile deformation in individual samples are apparently of similar grade to matrix assemblages (including GHS calc-silicate layers at the top of the Northern transect and the Everest Series samples collected by Wager above the East Rongbuk Glacier, Fig. 3, and on the Northeast Ridge of Mount Everest), implying that high temperatures close to those recorded in both mineral assemblages and deformation fabrics persisted through to the end of ductile deformation at each structural level – even if not for the whole shear zone at any given time (Waters, unpublished data).

We therefore favor scenario 3 in which the locus of deformation migrates up structural section during exhumation progressively accreting rocks that are penetratively deformed at lower and lower temperatures on to the upper margin of the shear zone, with microstructures and fabrics in the structurally lower and originally hotter parts of the shear zone being progressively frozen in as they are passively carried to shallower crustal levels. This is supported by the observations that deformation temperatures indicated by microstructures and fabric opening angles decrease up structural section in the Rongbuk transects (Fig. 10d–f and Fig. 13b) and that relatively large differential stresses are only supported at the highest structural positions (Fig. 13a) in the coolest rocks. As previously discussed by Cottle et al. (2011) for the Dzakaa Chu transect through the STDS, progressive accretion of cooler rocks during exhumation would result in progressive telescoping and translation of rocks deformed at different crustal depths and temperatures and the formation of a highly condensed section with an apparently smooth gradient in deformation temperatures.

4.6. Transport-direction parallel increase in telescoping of isotherms

In the three Rongbuk transects apparent thermal gradients increase traced southwards (Fig. 10) from the Northern transect (369 °C per km) through the Rongbuk Monastery transect (385 °C per km) to the Hermit's Gorge transect (420 °C per km). In contrast, as discussed in Section 3.8 above, Cottle et al. (2011) have estimated an apparent thermal gradient of ~310 °C per km for the Dzakaa Chu transect across the STDS, based on Raman spectroscopy of carbonaceous material and phase equilibria modeling. This transect is located some 50 km to the ENE of the Hermit's Gorge transect (Fig. 1). The projected positions of these four transects measured parallel to the transport direction indicated by stretching lineations in the GHS (Fig. 5) are shown in Fig. 18a, and apparent thermal gradients are plotted against position along the transport direction in Fig. 18b. Traced southwards, apparent thermal gradients increase slowly from the projected position of the Dzakaa Chu transect to the Northern transect and then progressively more rapidly through the Rongbuk Monastery to the Hermit's Gorge transect.

It is now accepted by many (but not all) Himalayan geologists that southward extrusion/exhumation of the GHS, which forms the crystalline core of the Himalaya, was driven by some form of channel flow in which the STDS forms the upper boundary of the channel, while the MCT forms the lower boundary (Fig. 2d; see reviews by Godin et al., 2006; Harris, 2007). If this extrusion involves a component of pure shear deformation and resultant transport-parallel stretching, as suggested by a number of recent vorticity studies of penetratively deformed GHS rocks both in the footwall to the STDS and the hanging wall to the MCT (e.g. Grasemann et al., 1999; Vannay and Grasemann, 2001; Law et al., 2004; Jessup et al., 2006; Larson and Godin, 2009; Larson et al., 2010a; Long et al., 2011; see also reviews in Langille et al., 2010; Wagner et al., 2010), then both the magnitude and rate of lateral extrusion must increase exponentially traced outward from the core of the orogen towards the foreland and syn-orogenic surface (Simpson and De Paor, 1997, p. 171; Williams et al., 2006, p. 226). This acceleration in magnitude and rate of lateral extrusion towards the foreland has obvious implications for deformation processes, including an increase in telescoping of isotherms, operating along both the upper (STDS) and lower (MCT) boundaries of the GHS.

However, although our data from the footwall to the STDS are certainly compatible with such extrusion models, caution should be applied in inferring lateral changes in thermal gradient from a series of such transects. For example, if the thermal profile is non-linear (e.g. highest thermal gradients at the STDS, becoming lower up and down section) then the average apparent thermal gradient on a long transect may be lower than on short local transects (cf. the 1200 m Dzakaa Chu transect described by Cottle et al., 2011, their Fig. 8, where gradient may be higher in the upper part of the transect, and the <550 m Rongbuk transects with linear gradients, Fig. 10). At the scale of the Greater Himalayan Slab (Fig. 2) vertical thermal profiles across the slab must be non-linear with thermal gradients decreasing towards the hotter, migmatic core of the GHS. If the STDS cuts progressively deeper in to the GHS traced down-dip to the north then, neglecting the additional influence of structural telescoping of isotherms, local thermal field gradients in the

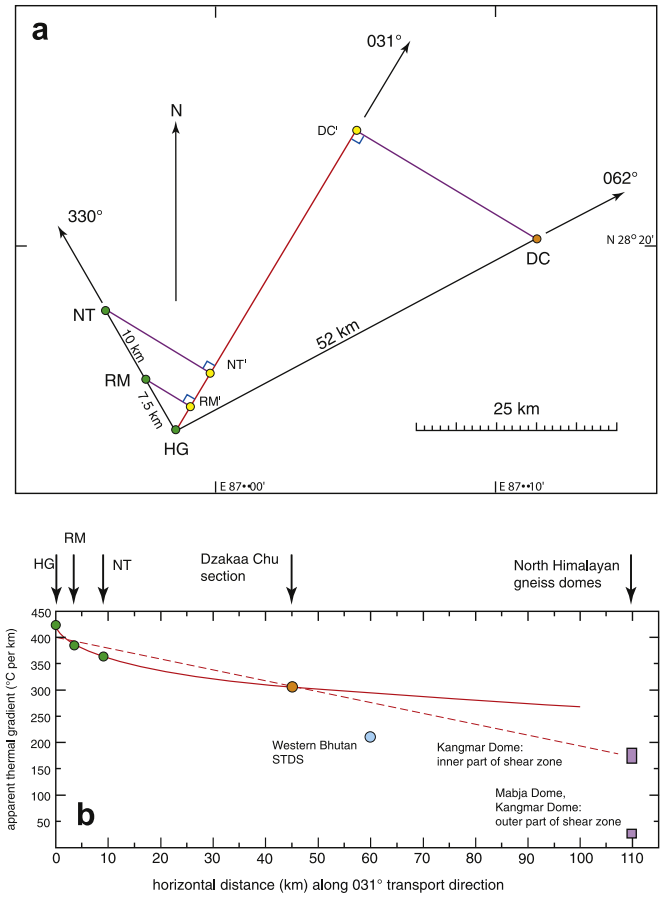

Fig. 18. (a) Map locations of the Hermit's Gorge (HG), Rongbuk Monastery (RMT) and Northern (NT) transects in relation to the Dzakaa Chu section (DC) through the South Tibetan Detachment System (STDS) described by Cottle et al. (2007, 2011). Projected positions of transects on a section line drawn through the Hermit's Gorge parallel to the 031° trending transport direction for the STDS (cf. Fig. 5) are indicated; projected position of Mabja Dome (Fig. 1) on this section line estimated at 110 km from Hermits Gorge, but not indicated in Fig. 18a. (b) Change in apparent thermal gradients associated with telescoping of isotherms/isograds traced along STDS transport direction. Apparent thermal gradients in Rongbuk transects (HG, RM, NT) based on deformation temperatures inferred from quartz fabric opening angles; Dzakaa Chu section based on peak temperatures indicated by phase equilibria modeling of metamorphic minerals, Raman spectroscopy of carbonaceous material and deformation temperatures indicated by microstructures (Cottle et al., 2011). Best-fit power law and linear regression lines to Rongbuk and Dzakaa Chu data indicated by solid and dashed lines, respectively. For comparison purposes, projected position of Kangmar Dome (Fig. 1) on section is assumed to be the same as that for Mabja Dome, while transects across klippen of the STDS in western Bhutan (Kellett et al., 2010) are placed ~50 km further towards foreland than Kangmar Dome. Apparent thermal gradients in western Bhutan transects based on phase equilibria modeling of metamorphic minerals (Kellett et al., 2010); gradients in Kangmar and Mabja Dome transects based on phase equilibria modeling and deformation temperatures indicated by microstructures (Wagner et al., 2010; Langille et al., 2010; Lee et al., 2000, 2004). Note different thermal gradients indicated by data of Wagner et al. (2010) for the inner (lower) and outer (higher) parts of the shear zone separating crystalline core of the Kangmar Dome from overlying Tethyan sedimentary rocks. See text for details.

immediate footwall to the STDS would still be expected to decrease traced towards the north.

4.7. Comparison with other transects across the STDS

Telescoping of inverted metamorphic isograds has been documented in a number of transects across the base of the GHS from Zanskar in the western Himalaya to Sikkim and Bhutan in the eastern Himalaya (Fig. 1) and related to reverse sense motion on the underlying MCT (e.g. Searle and Rex, 1989; Jain and Manickavasagam, 1993; Hubbard, 1996; Harrison et al., 1999; Searle et al., 1999; Stephenson et al., 2001). Inversion of peak metamorphic temperatures in Lesser Himalayan metasedimentary rocks located in the inferred footwall to the MCT of west-central Nepal and NW India (but cf. discussion by Searle et al., 2008 on structural position of MCT) has also been documented using Raman spectroscopy of carbonaceous material (e.g. Bollinger et al., 2004, 2006; Célérier et al., 2009), with peak metamorphic temperatures and apparent inverted thermal field gradients (30-20 °C per km; Célérier et al., 2009) decreasing from north to south. In contrast, there are only a relatively small number of field studies of telescoping of right way up isograds beneath the STDS at the top of the GHS. Both along the MCT and STDS, the majority of these studies are only qualitatively based on map spacing between isograds, and there are very few studies that have attempted to quantify the magnitude of telescoping based either on metamorphic isograds or on isotherms inferred from deformation features (e.g. recrystallization mechanisms, crystal fabrics) formed during shearing on the MCT or STDS.

In the eastern Himalaya of Bhutan steep apparent thermal field gradients have recently been described by Kellett et al. (2010) beneath klippen of the STDS (Fig. 1). Traced downward over a structural distance of 850 m, thermobarometry indicated peak metamorphic temperatures of ~600 °C in the Chekha Group (hanging wall to a lower strand of the STDS, probably the approximate lateral equivalent of the Lhotse detachment in the Everest region), increasing to ~780 °C at the base of a section of GHS rocks (footwall to STDS) with top-to-the-north shear sense indicators. The resultant apparent thermal field gradient (210 °C per km) is less steep than gradients estimated for either the Rongbuk transects (420-369 °C per km, based on quartz fabrics formed during top-to-the-north shearing) or the Dzakaa Chu section (310 °C per km, based on maximum metamorphic temperatures indicated by Raman spectroscopy of carbonaceous materials and phase equilibria modeling; Cottle et al., 2011). The foreland-hinterland positions of these Bhutan STDS sections relative to the Rongbuk and Dzakaa Chu sections are uncertain. Given their position some 50 km to the south and west of the North Himalayan gneiss domes (Fig. 1), this might indicate a slightly more hinterland position than the Dzakaa Chu section (Fig. 18b).

One of the first studies attempting to quantify both the magnitude of telescoping of isograds on the STDS, and the resultant implications for likely normal sense displacement, was reported by Herren (1987a, b) from the Zanskar Valley of the western Himalaya (Fig. 1). Here right way up isograds in the GHS are telescoped in to the overlying Zanskar shear zone, the westernmost strand of the STDS. In this study a homogenous simple shear model was employed to estimate likely magnitude of dip-slip displacement on the shear zone, based on measured orthogonal distances between biotite-garnet and sillimanite isograds outside (6.3 km) and inside (250 m) the shear zone. These distances correspond to a c. 96% apparent shortening between isograds, that is similar to the c. 90–94% apparent shortening indicated by the 0.5 km spacing between the projected positions of the 675 and 475 °C isotherms in the Rongbuk transects – see Section 4.1 for associated simplifying assumptions. Assuming that the observed telescoping of the isograds was due to homogenous simple shear in a 350 m wide shear zone inclined at 20° to the original isograds, Herren (1987a) estimated a minimum normal sense displacement of 25 km on the Zanskar shear zone.

This displacement estimate was questioned by Dèzes et al. (1999) who argued that, because of late stage thinning outside the main shear zone, the 6.3 km original orthogonal distance between isograds assumed in the Herren (1987a) analysis was an underestimate of the true distance. Hence, both the magnitudes of isograd telescoping and displacement on the shear zone estimated

by Herren (1987a) were too low. Dèzes et al. (1999) also argued that the Herren (1987a) analysis was particularly sensitive to both the assumed original angle (20°) between isograds and shear zone margins and small changes in the relative magnitudes of the shear zone width (350 m) and isograd spacing (250 m) within the shear zone that were estimated from field relationships. In their own study of the Zanskar shear zone, located c. 35–65 km along strike to the SE of the area described by Herren (1987a), Dèzes et al. (1999) used barometry data from metamorphic mineral assemblages in the GHS to estimate displacement on the shear zone, by assuming that exhumation occurred on particle paths that were parallel to the dip of the shear zone. Using the present day dip (~20°) of the shear zone in this area, Dèzes et al. (1999) estimated a minimum displacement of 35 ± 9 km on the shear zone. Walker et al. (1999) have also used structural data combined with P-T data and U–Pb geochronology to determine the geological evolution of the Zanskar shear zone. Assuming the original dip of the shear zone was similar to the present-day dip of 20–30° in the Zanskar valley, they estimated a displacement of 40–60 km on the Zanskar shear zone associated with Early Miocene age southward-directed extrusion of the GHS in the footwall to the shear zone.

However, Dèzes et al. (1999) have pointed out that due to large scale doming of the GHS in Zanskar the original dip of the shear zone was possibly less than its present dip of 20° and that, based on their barometry data, for an original dip of c. 12° the net dip-slip displacement on the Zanskar shear zone could have been as much as 100 ± 20 km. This would bring the estimated displacement to a similar magnitude as that later estimated by Searle et al. (2002, 2003, 2006), also based on barometry data, for the Everest transect through the STDS.

4.8. Comparison with North Himalayan gneiss domes

In the last decade the North Himalayan gneiss domes (also referred to as the South Tibetan gneiss domes), located approximately halfway between the Indus-Tsangpo suture to the north and the STDS to the south (Fig. 1), have been viewed by a number of researchers as erosional windows into the GHS that are located on the hinge of a large-scale antiform (e.g. Lee et al., 2000, 2004; Beaumont et al., 2001, 2004; Zhang et al., 2004; Larson et al., 2010a, b). In this interpretation (but cf. Aoya et al., 2006) the ductile shear zones separating Ordovician-Eocene sedimentary rocks (Tethyan Himalaya) from the underlying high grade metamorphic rocks exposed in the cores of these domes, are regarded as a direct continuation of the STDS exposed in the High Himalaya to the south and are closer to the presumed source of the underlying flowing channel. If correct, then is telescoping of metamorphic isograds and isothermal surfaces inferred from deformation fabrics also recorded in these shear zones, and how does the magnitude of telescoping compare with that observed on the STDS exposed to the south (Fig. 18b)? Here we should add that, although tectonically linked to the STDS exposed in the High Himalaya, the North Himalayan gneiss domes may be related to a different stage of orogen evolution and a different mechanism for exhumation of the mid-crust (e.g. channel flow models of Beaumont et al., 2004; Hodges, 2006). Therefore the thermal structure and strain patterns of the North Himalayan gneiss domes could be significantly different to the STDS.

For the Kangmar Dome (Fig. 1) deformation temperatures in mid-crustal mylonites separating the crystalline core from the overlying Tethyan sedimentary rocks have been estimated by Wagner et al. (2010) using mineral assemblages preserved in strain shadows of rotated porphyroclasts, quartz c-axis fabric opening angles, twinning mechanisms in calcite and recrystallization mechanisms in quartz and feldspar. Deformation temperatures decrease structurally upwards and isotherms are arched across the dome. Using the data shown by Wagner et al. (2010; their Fig. 5c) we estimate apparent thermal gradients over a total structural distance of approximately 3 km of c. 180 °C per km between their 650-450 °C isotherms, 160 °c per km between the 450-350 °C isotherms (Fig. 18b) and 24 °C per km gradient between the 350-300 °C isotherms. A similar microstructures- and crystal-fabrics-based analysis has been reported by Langille et al. (2010) for the Mabja Dome (Fig. 1) where estimated deformation temperatures steadily decrease up structural section from c. 650–700 °C (sillimanite zone) to 450–550 °C (chloritoid zone) over a structural distance of c. 8 km. In contrast to results from the Kangmar Dome, using the deformation temperature data shown by Langille et al. (2010; their Fig. 9) we estimate an average apparent thermal gradient of only c. 25 °C per km for the Mabja Dome (Fig. 18b).

However, although the apparent gradients in deformation temperatures for the Kangmar and Mabja domes are markedly different, field gradients in peak metamorphic pressures are similar. Lee et al. (2000) estimated an apparent gradient in pressure of 140 MPa per km for the Kangmar dome that, assuming an average rock density of 2700 g/m^3 (27 MPa/km), would indicate an 80% vertical shortening and (assuming pure shear deformation, but cf. vorticity data of Wagner et al., 2010) a 500% sub-horizontal stretching after the pressure gradient was "frozen in". For the Mabja Dome, Lee et al. (2004, p. 2311, data in right hand column) have estimated an apparent pressure gradient of 120–270 MPa per km (between the chloritoid-in isograd and garnet zone rocks), indicating vertical shortening of 75–90% and (once again assuming pure shear deformation, but cf. vorticity data of Langille et al., 2010), resultant horizontal stretches of 400–1000%. The similarities in vertical shortening inferred from apparent pressure gradients in the Kangmar and Majba domes (80 and 75–90%, respectively), lead us to speculate that the major differences in apparent deformation temperature gradients may be due to when the deformation fabrics were "frozen in" during vertical shortening and progressive exhumation. We suggest that the 650-c. 350 °C deformation fabrics in the Kangmar Dome may have been frozen in during the early stages of vertical thinning at close to peak metamorphic temperatures – as previously concluded by Wagner et al. (2010, p. 19) based on the observation that deformation temperatures overlap with peak metamorphic temperatures estimated by Lee et al. (2000). For the Mabja Dome (and the 350-300 °C Kangmar rocks) we suggest that deformation fabrics were frozen in at a relatively late stage of vertical thinning, after the thermal structure had relaxed towards a normal geothermal gradient. This is compatible with the suggestion by Lee et al. (2004, p. 2311) that peak metamorphic pressures and temperatures in Mabja occurred at different times, and the observation of Langille et al. (2010, p. 80) that deformation temperatures (at least in the upper part of the section) were cooler than peak metamorphic temperatures.

In summary, we suggest that the degree of telescoping of isotherms/isograds around the margins of at least two of the North Himalayan gneiss domes (for which appropriate data are available) bears a striking similarity to the telescoping documented along the STDS in the Himalaya to the south and west of these domes (Fig. 18b).

5. Conclusions

Integrated microstructural and quartz c-axis fabric analyses of Greater Himalayan Series (GHS) samples collected along three transects at distances of 10–550 m beneath the South Tibetan Detachment in the Rongbuk area to the north of Mount Everest leads to the following conclusions.

1. Microstructures and quartz c-axis fabrics developed during top down to the N shearing associated with southwards directed extrusion/exhumation of the GHS rocks.
2. Deformation temperatures indicated by quartz c-axis fabric opening angles in the metasedimentary rocks range from 490 to 680 °C, and increase linearly with depth beneath the detachment along each transect. Isothermal surfaces projected between the three transects are sub-parallel to the sheet dip of GHS foliation. These isothermal surfaces also strike sub-parallel to the overlying detachment, but dip at c. 10° less steeply towards the NE.
3. Deformation temperatures indicated by fabric opening angles in thin (10–20 cm) pervasively deformed leucogranite sills are similar to adjacent metasedimentary rocks indicating that they cooled to ambient background temperatures before penetrative deformation ceased. In contrast, deformation temperatures in thicker sills are always higher than in adjacent metasedimentary rocks suggesting that they had not cooled to ambient temperatures (c. 525–550 °C) when plastic deformation of quartz ceased and fabrics were 'locked in'. This in turn suggests that the leucogranites were intruded during a relatively late stage of penetrative deformation associated with exhumation.
4. Recrystallized quartz grain size piezometry indicates differential flow stresses of 10–15 MPa in the metasedimentary rocks at 100–550 m beneath the detachment, increasing to 25–35 MPa in the cooler rocks at $<$ 50 m beneath the detachment. Flow stress and deformation temperature data indicate strain rates of 10^{-13} to 10^{-14} s^{-1} (Hirth et al., 2001 flow law) in metasedimentary rocks at 550–100 m beneath the STDS, increasing to strain rates of 10^{-12} s^{-1} at $<$ 50 m beneath the detachment. For individual samples, the flow law of Rutter and Brodie (2004) indicates strain rates one to two orders of magnitude slower than the Hirth et al. (2001) flow law, depending on structural position.
5. Traced from north to south, linear regression of deformation temperature data from the metasedimentary rocks indicates apparent thermal gradients of 369, 385 and 420 °C per km along the three Rongbuk sampling transects. These apparent thermal gradients are of similar magnitude to a metamorphic field gradient of ~310 °C per km described by Cottle et al. (2011) from the Dzakaa Chu section across the STDS, located 50 km to the ENE of the Rongbuk area and based on Raman spectroscopy of carbonaceous material and phase equilibria modeling. The similar apparent thermal gradients across the STDS on the Dzakaa Chu section and Rongbuk transects provides strong supporting evidence that measured quartz fabric opening angles from the Rongbuk transects are primarily controlled by deformation temperature rather than strain rate or hydrolytic weakening.
6. Observed telescoping of deformation temperatures on the Rongbuk transects could be due to penetrative strain associated with extreme vertical thinning (pure shear model). Vertical penetrative thinning – assuming horizontal geotherms and geothermal gradients of 40-25 °C per km during plane strain deformation, requires shortening of 90–94%% and strain ratios of between 100:1 and 250:1 measured in XZ sections, for which there is no supporting field or microstructural evidence. Nonetheless, the apparent shortening indicated by telescoping of isotherms on the Rongbuk transects is closer similar to previously published estimates of apparent shortening on the westernmost strand of the STDS in Zanskar (96% based on telescoping of isograds that predate shearing) and in two of the North Himalayan gneiss domes (80 and 75–90% based on barometry data) located to the north and northeast of the Rongbuk area.
7. We have explored several alternative models in which telescoping of deformation temperatures on the Rongbuk transects was caused by downward increasing transport of material during penetrative flow associated with southwards extrusion/exhumation of the GHS (heterogeneous simple or general shear models) as assumed, for example, in channel flow models. In these differential flow path models we favor a scenario in which the locus of deformation migrates up structural section during exhumation, progressively accreting rocks that were penetratively deformed at lower and lower temperatures on to the upper margin of the shear zone, with microstructures and fabrics in the structurally lower and originally hotter parts of the shear zone being progressively frozen in as they are passively carried to shallower crustal levels.
8. Using sections drawn parallel to the local transport direction for the STDS these highly simplified differential flow path models indicate that detachment-parallel transport magnitudes of 25–170 km are needed to explain the telescoping of isotherms in the immediate footwall to the STDS, depending on assumed original geothermal gradient, dip of detachment etc. These displacement estimates are in broad agreement with previously published estimates for dip-slip displacement on the STDS (90–216 km) based on barometry data from GHS rocks in the Everest region, and are at least compatible with channel flow models for southward-directed extrusion and exhumation of the GHS. However, these displacement estimates are more difficult to reconcile with tectonic models in which the GHS was transported southwards on underlying thrusts, with the STDS playing only a minor role in extrusion/exhumation of the GHS.
9. Previously published vorticity analyses indicate that penetrative deformation on the Rongbuk transects involved significant components (62-20%) of pure shear deformation. If extrusion of the GHS involved a component of pure shear deformation and resultant transport-parallel stretching, then both the magnitude and rate of lateral extrusion must increase exponentially traced outward from the core of the orogen towards the foreland, resulting in a southward increase in telescoping of isotherms. This is compatible with our observations that traced southwards in the Everest region, telescoping of isotherms/isograds in the footwall to the STDS increases from ~310 °C per km on the Dzakaa Chu section to 369, 385 and finally 420 °C per km along the three Rongbuk transects.

Acknowledgments

This work was funded by National Science Foundation grants EAR 0207524 and EAR 0711207 to R.D. Law and M.P. Searle. M.K. Francsis gratefully acknowledges scholarship support from ConocoPhillips. Bernhard Grasemann is thanked for suggesting the particle path model (Fig. 15) as a potential mechanism for telescoping of isotherms in the footwalls to detachments. We thank Djordje Grujic, Paris Xypolias and Jeff Lee for their reviews and constructive comments on the manuscript, and Bob Holdsworth for editorial handling. We also thank Tashi Sherpa for help with sample collecting. RDL also thanks Sean Mulcahy and Neil Mancktelow for software packages facilitating collection and analysis of universal stage data, and Evelin Herren for discussion on her Zanskar shear zone work.

Appendix. Supplementary material

Supplementary data associated with this article can be found in the online version, at doi:10.1016/j.jsg.2011.09.004.

References

Aoya, M., Wallis, S.R., Kawakami, T., Lee, J., Wang, Y., Maesa, H., 2006. The Malashan gneiss-dome in south Tibet: comparative study with the Kangmar dome with special reference to kinematics of deformation and origin of associated granites. In: Law, R.D., Searle, M.P., Godin, L. (Eds.), Channel Flow, Ductile Extrusion and Exhumation in Continental Collision Zones. Geological Society of London, Special Publication, vol. 268 pp. 471–495.

Beaumont, C., Jamieson, R.A., Nguyen, M.H., Lee, B., 2001. Himalayan tectonics explained by extrusion of a low-viscosity crustal channel coupled to focused surface denudation. Nature 414, 738–742.

Beaumont, C., Jamieson, R.A., Nguyen, M.H., Medvedev, S., 2004. Crustal channel flows: 1 Numerical models with applications to the tectonics of the Himalayan-Tibetan orogen. Journal of Geophysical Research – Solid Earth 109, B06406.

Bollinger, L., Avouac, J.P., Beyssac, O., Catlos, E.J., Harrison, T.M., Grove, M., Goffé, B., Sapkota, S., 2004. Thermal structure and exhumation history of the Lesser Himalaya in central Nepal. Tectonics 23, TC5015. doi:10.1029/2003TC001564.

Bollinger, L., Henry, P., Avouac, J.P., 2006. Mountain building in the Nepal Himalaya: thermal and kinematic model. Earth and Planetary Science Letters 244, 58–71.

Burchfiel, B.C., Zhiliang, C., Hodges, K.V., Yuping, L., Royden, L., Changrong, D., Jiene, X., 1992. The South Tibetan Detachment System, Himalayan Orogen: extension contemporaneous with and parallel to shortening in a collisional mountain belt. Geological Society of America Special Paper 269, 41.

Carosi, R., Lombardo, B., Molli, G., Musumeci, G., Pertusati, P., 1998. The South Tibetan detachment system in the Rongbuk valley, Everest region. Deformation features and geological implications. Journal of Asian Earth Sciences 16, 299–311.

Célérier, J., Harrison, T.M., Beyssac, O., Herman, F., Dunlap, W.J., Webb, A.G., 2009. Evolution of the Kumaun and Garwhal Lesser Himalaya, India. Part 2: thermal and deformation histories. Geological Society of America Bulletin 121, 1281–1297.

Cottle, J.M., 2007. Timing of crustal metamorphism, melting and exhumation of the Greater Himalayan crust, Makalu-Kangshung-Kharta region, south Tibetan Himalaya, Ph.D. thesis: Oxford, University of Oxford, 277 p.

Cottle, J.M., Jessup, M.J., Newell, D.L., Searle, M.P., Law, R.D., Horstwood, M.S.A., 2007. Structural insights into the early stages of exhumation along an orogen-scale detachment: the South Tibetan Detachment System, Dzakaa Chu section, Eastern Himalaya. Journal of Structural Geology 29, 1781–1797. doi:10.1016/j.jsg.2007.08.007.

Cottle, J.M., Searle, M.P., Horstwood, M.S.A., Waters, D.J., 2009. Timing of mid-crustal metamorphism, melting and deformation in the Mount Everest Region of Southern Tibet revealed by U (-Th) -Pb geochronology. Journal of Geology 117, 643–664. doi:10.1086/605994.

Cottle, J.M., Waters, D.J., Riley, D., Beyssac, O., Jessup, M.J., 2011. Metamorphic history of the south Tibetan detachment system, Mt. Everest region, revealed by RSCM thermometry and phase equilibria modeling. Journal of Metamorphic Geology 29, 561–582. doi:10.1111/j.1525-1314.2011.00930.x.

Dèzes, P.J., Vannay, J.-C., Steck, A., Bussy, F., Cosca, M., 1999. Synorogenic extension, quantitative constraints on the age and displacement of the Zanskar Shear Zone (northwest Himalaya). Geological Society of America Bulletin 111, 364–374.

Fitzgerald, J.D., Stunitz, H., 1993. Deformation of granitoids at low metamorphic grade. I: reactions and grain size reduction. Tectonophysics 221, 269–297.

Godin, L., Grujic, D., Law, R.D., Searle, M.P., 2006. Channel flow, ductile extrusion and exhumation in continental collision zones: an introduction. In: Law, R.D., Searle, M.P., Godin, L. (Eds.), Channel Flow, Ductile Extrusion and Exhumation in Continental Collision Zones. Geological Society of London, Special Publication, vol. 268 pp. 1–23.

Grasemann, B., Mancktelow, N.S., 1993. Two dimensional thermal modeling of normal faulting: the Simplon fault zone, central Alps, Switzerland. Tectonophysics 225, 155–165.

Grasemann, B., Fritz, H., Vannay, J.-C., 1999. Quantitative kinematic flow analysis from the Main Central Thrust Zone (NW-Himalaya, India): implications for a decelerating strain path and the extrusion of orogenic wedges. Journal of Structural Geology 21, 837–853.

Grujic, D., Hollister, L.S., Parrish, R.R., 2002. Himalayan metamorphic sequence as an orogenic channel: insight from Bhutan. Earth and Planetary Science Letters 198, 177–191.

Grujic, D., Stipp, M., Wooden, J.L., 2009. Thermometry of quartz in mylonites (abstract). Goldschmidt Conference 2009. Geochimica Cosmochim Acta 73 (13), A-472. doi:10.1016/g.gca.2009.05.025. Supplement 1.

Grujic, D., Stipp, M., Wooden, J.L., 2011. Thermometry of quartz mylonites: importance of dynamic recrystallization on Ti-in-quartz reequilibration. Geochemistry, Geophysics, Geosystems G3 (12), Q06012. doi:10.1029/2010GC003368.

Harris, N., 2007. Channel flow and the Himalayan – Tibetan orogen: a critical review. Journal of the Geological Society of London 164, 511–523.

Harrison, T.M., Grove, M., Lovera, O.M., Catlos, E.J., D'Andrea, J., 1999. The origin of Himalayan anatexis and inverted metamorphism: models and constraints. Journal of Asian Earth Sciences 17, 755–772.

Herren, E., 1987a. Zanskar shear zone: northeast-southwest extension within the Higher Himalayas (Ladakh, India). Geology 15, 409–413.

Herren, E., 1987b. Structure, deformation and metamorphism of the Zanskar area, Ladakh Himalaya, NW India, Ph.D. thesis: Swiss Federal Institute of Technology, Zurich.

Hirth, G., Tullis, J., 1992. Dislocation creep regimes in quartz aggregates. Journal of Structural Geology 14, 145–159.

Hirth, G., Teyssier, C., Dunlap, W.J., 2001. An evaluation of quartzite flow laws based on comparisons between experimentally and naturally deformed rocks. International Journal of Earth Sciences 90, 77–87.

Hodges, K.V., 2006. A synthesis of the Channel Flow – Extrusion hypothesis as developed for the Himalayan – Tibet orogenic system. In: Law, R.D., Searle, M.P., Godin, L. (Eds.), Channel Flow, Ductile Extrusion and Exhumation in Continental Collision Zones. Geological Society of London, Special Publication, vol. 268 pp. 71–90.

Hodges, K.V., Parrish, R.R., Housh, T.B., Lux, D.R., Burchfiel, B.C., Royden, L.H., Chen, Z., 1992. Simultaneous Miocene extension and shortening in the Himalayan orogen. Science 258, 1466–1470.

Hodges, K.V., Bowring, S., Davidek, K., Hawkins, D., Krol, M., 1998. Evidence for rapid displacement on Himalayan normal faults and the importance of tectonic denudation in the evolution of mountain ranges. Geology 26, 483–486.

Hodges, K.V., Hurtado, J.M., Whipple, K.X., 2001. Southward extrusion of Tibetan crust and its effect on Himalayan tectonics. Tectonics 20, 799–809.

Holyoke, C.W., Kronenberg, A.K., 2010. Accurate differential stress measurement using the molten salt cell and solid salt assemblies in the Griggs apparatus with application to strength piezometers and rheology. Tectonophysics 494, 17–31.

Hubbard, M., 1996. Ductile shear as a cause of inverted metamorphism: example from the Nepal Himalaya. Journal of Geology 104, 493–499.

Jain, A.K., Manickavasagam, R.M., 1993. Inverted metamorphism in the intercontinental ductile shear zone during Himalayan collision tectonics. Geology 21, 407–410.

Jessup, M.J., Law, R.D., Searle, M.P., Hubbard, M.S., 2006. Structural evolution and vorticity of flow during extrusion and exhumation of the Greater Himalayan Slab, Mount Everest Massif, Tibet/Nepal: implications for orogen-scale flow partitioning. In: Law, R.D., Searle, M.P., Godin, L. (Eds.), Channel Flow, Extrusion, and Exhumation in Continental Collision Zones. Geological Society of London, Special Publication, vol. 268, pp. 379-414.

Jessup, M.J., Cottle, J.M., Searle, M.P., Law, R.D., Newell, D.L., Tracy, R.J., Waters, D.J., 2008. PT-t-D paths of Everest Series schist, Nepal. Journal of Metamorphic Geology 26, 717–739.

Kellett, D.A., Grujic, D., Warren, C., Cottle, J., Jamieson, R., Tenzin, T., 2010. Metamorphic history of a syn-convergent orogen-parallel detachment: the South Tibetan detachment system, Bhutan Himalaya. Journal of Metamorphic Geology 28, 785–808.

Kohn, M.J., 2008. P-T-t data from central Nepal support critical taper and repudiate large-scale channel flow of the Greater Himalayan Sequence. Geological Society of America Bulletin 120, 259–273.

Kohn, M.J., Northrup, C.J., 2009. Taking mylonites' temperatures. Geology 37, 47–50.

Kronenberg, A.K., Wolf, G.H., 1990. Fourier transform infrared spectroscopy determinations of intragranular water content in quartz-bearing rocks: implications for hydrolytic weakening in the laboratory and within the earth. Tectonophysics 172, 255–271.

Kruhl, J.H., 1998. Reply: prism- and basal-plane parallel subgrain boundaries in quartz: a microstructural geothermobarometer. Journal of Metamorphic Geology 16, 142–146.

Langille, J., Lee, J., Hacker, B., Seward, G., 2010. Middle crustal ductile deformation patterns in southern Tibet: insights from vorticity studies in Mabja Dome. Journal of Structural Geology 32, 70–85.

Larson, K.P., Godin, L., 2009. Kinematics of the Greater Himalayan Sequence, Dhaulagiri Himal: implications for the structural framework of central Nepal. Journal of the Geological Society of London 166, 25–43.

Larson, K.P., Godin, L., Price, R.A., 2010a. Relationship between displacement and distortion in orogens: linking the Himalayan foreland and hinterland in Central Nepal. Geological Society of America Bulletin 122, 1116–1134.

Larson, K.P., Godin, L., Davis, W.J., Davis, D.W., 2010b. Out-of-sequence deformation and expansion of the Himalayan orogenic wedge: insight from the Changgo culmination, south central Tibet. Tectonics 29, TC4013. doi:10.1029/2008TC002393.

Law, R.D., 2010. Moine thrust zone mylonites at the Stack of Glencoul: II – results of vorticity analyses and their tectonic significance. In: Law, R.D., Butler, R.W.H., Holdsworth, R., Krabbendam, M., Strachan, R. (Eds.), Continental Tectonics and Mountain Building – The Legacy of Peach and Horne. Geological Society, London, Special Publication, vol. 335, pp. 579–602.

Law, R.D., Morgan, S.S., Casey, M., Sylvester, A.G., Nyman, M., 1992. The Papoose Flat pluton of eastern California: a re-assessment of its emplacement history in the light of new microstructural and crystallographic fabric observations. Transactions Royal Society Edinburgh. Earth Sciences 83, 361–375.

Law, R.D., Searle, M.P., Simpson, R.L., 2004. Strain, deformation temperatures and vorticity of flow at the top of the Greater Himalayan Slab, Everest massif, Tibet. Journal of the Geological Society of London 161, 305–320.

Law, R.D., Searle, M.P., Godin, L., 2006. Channel Flow, Ductile Extrusion and Exhumation in Continental Collision Zones, vol. 268. Geological Society of London. Special Publication, 620 p.

Law, R.D., Jessup, M.J., Searle, M.P., Cottle, J.M., Waters, D., 2008. Telescoping of isotherms beneath the south Tibetan detachment, Mount Everest massif: implications for magnitude of internal flow during extrusion of the Greater Himalayan Slab (extended abstract). 23rd annual Himalayan-Karakoram-Tibet Workshop. Himalayan Journal of Earth Sciences 5 (7), 86–87.

Law, R.D., Stahr, D., Grasemann, B., Ahmad, T., 2011. Deformation temperatures and flow vorticities near the base of the Greater Himalayan Crystalline Sequence, Sutlej valley and Shimla Klippe, NW India (abstract). Geophysical Research

Abstracts 13, EGU2011–2300. European Geophysical Union General Assembly 2011.
Lee, J., Hacker, B.R., Wang, Y., 2000. Evolution of the North Himalayan gneiss domes: structural and metamorphic studies in Mabja Dome, southern Tibet. Journal of Structural Geology 26, 2297–2316.
Lee, J., Hacker, B.R., Dinklage, W.S., Wang, Y., Gans, P., Calvert, A., Wan, J., Chen, W., Blythe, A., McClelland, W., 2004. Evolution of the Kangmar Dome, southern Tibet: structural, petrologic, and thermochronologic constraints. Tectonics 19, 872–895.
Lister, G.S., 1977. Crossed-girdle c-axis fabrics in quartzites plastically deformed by plane strain and progressive simple shear. Tectonophysics 39, 51–54.
Lister, G.S., Dornsiepen, U.F., 1982. Fabric transitions in the Saxony Granulite Terrain. Journal of Structural Geology 4, 81–92.
Lister, G.S., Hobbs, B.E., 1980. The simulation of fabric development during plastic deformation and its application to quartzite: the influence of deformation history. Journal of Structural Geology 2, 355–370.
Lister, G.S., Williams, P.F., 1979. Fabric development in shear zones: theoretical controls and observed phenomena. Journal of Structural Geology 1, 283–298.
Lombardo, B., Pertusati, P., Borgi, S., 1993. Geology and tectonomagmatic evolution of the eastern Himalaya along the Chomolungma – Makalu transect. In: Treloar, P.J., Searle, M.P. (Eds.), Himalayan Tectonics, Geological Society London, Special Publication, vol. 74, pp. 341–55.
Long, S., McQuarri, N., Tobgay, T., Hawthorne, J., 2011. Quantifying internal strain and deformation temperature in the eastern Himalaya, Bhutan; Implications for the evolution of strain in thrust sheets. Journal of Structural Geology 33, 579–608.
Means, W.D., 1995. Shear zones and rock history. Tectonophysics 247, 157–160.
Morgan, S.S., Law, R.D., 2004. Unusual transition in quartzite dislocation creep regimes and crystal slip systems in the aureole of the EJB pluton, California: a case for anhydrous conditions created by decarbonation of adjacent marbles. Tectonophysics 384, 209–231.
Murphy, M.A., Harrison, T.M., 1999. Relationship between leucogranites and the Qomolangma detachment in the Rongbuk valley, south Tibet. Geology 27, 831–834.
Myrow, P.M., Hughes, N.C., Searle, M.P., Fanning, C.M., Peng, S.-C., Parcha, S.K., 2009. Stratigraphic correlation of Cambrian-Ordovician deposits along the Himalaya: implications for the age and nature of rocks in the Mount Everest region. Geological Society of America Bulletin 120, 323–332.
Pfiffner, O.A., Ramsay, J.G., 1982. Constraints on geological strain rates, arguments from finite strain states of naturally deformed rocks. Journal of Geophysical Research 87, 311–321.
Pognante, U., Benna, P., 1993. Metamorphic zonation, migmatization and leucogranites along the Everest transect of eastern Nepal and Tibet: record of an exhumation history. In: Treloar, P.J., Searle, M.P. (Eds.), Himalayan Tectonics. Geological Society, London, Special Publication, vol. 74, pp. 323–40.
Robinson, D.M., DeCelles, P.G., Copeland, P., 2006. Tectonic evolution of the Himalayan thrust belt in western Nepal: implications for channel flow models. Geological Society of America Bulletin 118, 865–885.
Rutter, E.H., Brodie, K., 2004. Experimental intracrystalline plastic flow in hot-pressed synthetic quartzite prepared from Brazilian quartz crystals. Journal of Structural Geology 26, 259–270.
Sakai, S., Sawada, M., Takigami, Y., Orihasi, Y., Danhara, T., Iwano, H., Kuwahara, Y., Dong, Q., Li, J., 2005. Geology of the summit limestone of Mount Qomolangma (Everest) and cooling history of the Yellow Band under the Qomolangma detachment. The Island Arc 14, 297–310.
Searle, M.P., 1999. Extensional and compressional faults in the Everest-Lhotse massif, Khumbu Himalaya, Nepal. Journal of the Geological Society of London 156, 227–240.
Searle, M.P., 2003. Geological Map of the Mount Everest Region, Nepal and South Tibet; Scale 1:50,000. Department of Earth Sciences, Oxford University, U.K.
Searle, M.P., Rex, A.J., 1989. Thermal model for the Zanskar Himalaya. Journal of Metamorphic Geology 7, 127–134.
Searle, M.P., Waters, D.J., Dransfield, M.W., Stephenson, B.J., Walker, C.B., Walker, J.D., Rex, D.C., 1999. Thermal and mechanical models for the structural evolution of Zanskar High Himalaya. In: MacNiocaill, C., Ryan, P.D. (Eds.), Continental Tectonics. Geological Society of London, Special Publication, vol. 164, pp. 139–156.
Searle, M.P., Simpson, R.L., Law, R.D., Waters, D.J., Parrish, R.R., 2002. Quantifying displacement on the South Tibetan Detachment normal fault, Everest massif, and the timing of crustal thickening and uplift in the Himalaya and Tibet. Journal of Nepal Geological Society 26, 1–6.
Searle, M.P., Simpson, R.L., Law, R.D., Parrish, R.R., Waters, D.J., 2003. The structural geometry, metamorphic and magmatic evolution of the Everest massif, High Himalaya of Nepal-South Tibet. Journal of the Geological Society of London 160, 344–366.
Searle, M.P., Law, R.D., Jessup, M.J., 2006. Crustal structure, restoration and evolution of the Greater Himalaya in Nepal-South Tibet; implications for channel flow and ductile extrusion of the middle crust. In: Law, R.D., Searle, M.P., Godin, L. (Eds.), Channel Flow, Ductile Extrusion and Exhumation in Continental Collision Zones. Geological Society of London, Special Publication, vol. 268 pp. 355–378.
Searle, M.P., Stephenson, B., Walker, J., Walker, C., 2007. Restoration of the Western Himalaya: implications for metamorphic protoliths, thrust and normal faulting, and channel flow models. Episodes 30, 242–257.
Searle, M.P., Law, R.D., Godin, L., Larson, K.P., Streule, M.J., Cottle, J.M., Jessup, M.J., 2008. Defining the Himalayan Main Central thrust in Nepal. Journal of the Geological Society of London 165, 523–534.
Sibson, R.H., 1977. Fault rocks and fault mechanisms. Journal of the Geological Society of London 133, 191–213.
Simpson, C., De Paor, D.G., 1997. Practical analysis of general shear zones using porphyroclast hyperbolic distribution method: an example from the Scandinavian Caledonides. In: Sengupta, S. (Ed.), Evolution of Geological Structures in Micro- to Macro-scales. Chapman and Hall, London, pp. 169–184.
Stephenson, B.J., Searle, M.P., Waters, D.J., Rex, D.C., 2001. Structure of the main central thrust zone and extrusion of the high Himalayan deep crustal wedge, Kishtwar-Zanskar Himalaya. Journal of the Geological Society of London 158, 637–652.
Stipp, M., Stunitz, H., Heilbronner, R., Schmid, S., 2002a. Dynamic recrystallization of quartz: correlation between natural and experimental conditions. In: De Meer, S., Drury, M.R., De Bresser, J.H.P., Pennock, G.M. (Eds.), Deformation Mechanisms, Rheology and Tectonics: Current Status and Future Perspectives. Geological Society of London, Special Publication, vol. 200, pp. 171–190.
Stipp, M., Stunitz, H., Heilbronner, R., Schmid, S., 2002b. The eastern Tonale fault zone: a natural laboratory for crystal plastic deformation of quartz over a temperature range from 250 to 700 °C. Journal of Structural Geology 24, 1861–1884.
Stipp, M., Tullis, J., 2003. The recrystallized grain size piezometer for quartz. Geophysical Research Letters 2088. doi:10.1029/2003GL018444.
Stipp, M., Tullis, J., Behrens, H., 2006. Effect of water on the dislocation creep microstructure and flow stress of quartz and implications for the recrystallized grain size piezometer. Journal of Geophysical Research 111, B042201. doi:10.1029/2005JB003852.
Stipp, M., Tullis, J., Scherwath, M., Behrmann, J.H., 2010. A new perspective on paleopiezometry: dynamically recrystallized grain size distributions indicate mechanism changes. Geology 38, 759–762. doi:10.1130/G31162.1.
Thomas, J.B., Watson, E.B., Spear, F.S., Shemella, P.T., Nayak, S.K., Lanzirotti, A., 2010. TitaniQ under pressure: the effect of pressure and temperature on the solubility of Ti in quartz. Contributions to Mineralogy and Petrology doi:10.007/s00410-010-0503-3.
Tullis, J.A., Yund, R.A., 1992. The brittle-ductile transition in feldspar aggregates: an experimental study. In: Evans, B., Wong, T.F. (Eds.), Fault Mechanics and Transport Properties of Rocks. Academic Press, London, pp. 89–117.
Tullis, J.A., Christie, J.M., Griggs, D.T., 1973. Microstructures and preferred orientations of experimentally deformed quartzites. Geological Society of America Bulletin 84, 297–314.
Vannay, J.-C., Grasemann, B., 2001. Himalayan inverted metamorphism and syn-convergence extension as a consequence of a general shear extrusion. Geological Magazine 138, 253–276.
Wagner, T., Lee, J., Hacker, B.R., Seward, G., 2010. Kinematics and vorticity in Kangmar Dome, southern Tibet: testing midcrustal channel flow models for the Himalaya. Tectonics 29, TC6011,. doi:10.1029/2010TC002746.
Walker, J.D., Martin, M.W., Bowring, S.A., Searle, M.P., Waters, D.J., Hodges, K.V., 1999. Metamorphism, melting and extension: age constraints from the High Himalayan slab of Southeastern Zanskar and northwest Lahaul. Journal of Geology 107, 473–495.
Wallis, S.R., 1992. Vorticity analysis in a metachert from the Sanbagawa belt, SW Japan. Journal of Structural Geology 14, 271–280.
Wallis, S.R., 1995. Vorticity analysis and recognition of ductile extension in the Sanbagawa belt, SW Japan. Journal of Structural Geology 17, 1077–1093.
Wark, D.A., Watson, E.B., 2006. The TitaniQ: a Titanium in quartz geothermometer. Contributions to Mineralogy and Petrology 152, 743–754.
Waters, D.J., Law, R.D., Searle, M.P., 2006. Metamorphic evolution of the upper parts of the Greater Himalayan Slab, Everest area, from the 1933 sample collection of L. R. Wager (abstract). Journal of Asian Earth Sciences 26, 168. 21st annual Himalayan-Karakoram-Tibet Workshop.
Williams, P.F., Jiang, D., Lin, S., 2006. Interpretation of deformation fabrics of infrastructure zone rocks in the context of channel flow and other tectonic models. In: Law, R.D., Searle, M.P., Godin, L. (Eds.), Channel Flow, Ductile Extrusion and Exhumation in Continental Collision Zones. Geological Society London, Special Publication, vol. 268, pp. 221–236.
Yin, A., 2006. Cenozoic tectonic evolution of the Himalayan orogen as constrained by along-strike variation of structural geometry, exhumation history, and foreland sedimentation. Earth Science Reviews 76, 1–131.
Yin, C.H., Kuo, S.T., 1978. Stratigraphy of the Mount Jolmo Lungma and its north slope. Scientia Sinica 21, 629–644.
Zhang, H., Harris, N., Parrish, R.R., Kelley, S., Zhang, L., Rogers, N., Argles, T., King, J., 2004. Causes and consequences of protracted melting of mid-crust exposed in the North Himalayan Antiform. Earth and Planetary Science Letters 228, 195–212. doi:10.1016/j.epsl.2004.09.031.